

# Scenario Choice Impacts Carbon Allocation Projection at Global Warming Levels

Lee de Mora<sup>1</sup>, Ranjini Swaminathan<sup>2</sup>, Richard P. Allan<sup>2</sup>, Jeremy Blackford<sup>1</sup>, Douglas I. Kelley<sup>3</sup>, Phil Harris<sup>3</sup>, Chris D. Jones<sup>4</sup>, Colin G. Jones<sup>5</sup>, Spencer Liddicoat<sup>4</sup>, Robert J. Parker<sup>6,7</sup>, Tristan Quaife<sup>2</sup>, Jeremy Walton<sup>4</sup>, and Andrew Yool<sup>8</sup>

<sup>1</sup>Plymouth Marine Laboratory, Plymouth, PL1 3DH

<sup>2</sup>National Centre for Earth Observation and Department of Meteorology, University of Reading, Reading, UK

<sup>3</sup>UK Centre for Ecology & Hydrology, Wallingford, Oxfordshire, OX10 8BB, UK

<sup>4</sup>Met Office Hadley Centre for Climate Science and Services, Exeter, EX1 3PB, UK

<sup>5</sup>National Centre for Atmospheric Science, UK, and School of Earth and Environment, University of Leeds, Leeds, UK

<sup>6</sup>National Centre for Earth Observation, Space Park Leicester, University of Leicester, Leicester, UK

<sup>7</sup>Earth Observation Science, School of Physics and Astronomy, University of Leicester, UK

<sup>8</sup>National Oceanography Centre, European Way, Southampton, SO14 3ZH, UK

**Correspondence:** Lee de Mora (ledm@pml.ac.uk)

## Abstract.

We show that the distribution of anthropogenic carbon between the atmosphere, land surface and ocean differs with the choice of projection scenario even for identical changes in mean global surface temperature. Warming thresholds occur later in lower [carbon dioxide \(CO<sub>2</sub>\)](#) emissions scenarios and with less carbon in the three main reservoirs than in higher CO<sub>2</sub> emissions scenarios. At 2 °C of warming, the mean carbon allocation differs by up to [6263](#) PgC between scenarios and this is equivalent to approximately six years of ~~our~~ current global total emissions. [At the same warming level, higher CO<sub>2</sub> concentration scenarios have a lower combined ocean and land carbon allocation fraction of the total carbon compared to lower CO<sub>2</sub> concentration scenarios.](#)

The warming response to ~~carbon dioxide, included via~~ [CO<sub>2</sub>, quantified as](#) the equilibrium climate sensitivity, ECS, directly impacts ~~the a models~~ global warming threshold exceedance year and [hence](#) the carbon allocation. Low ECS models have more ~~total~~ carbon than high ECS models at a given warming level because the warming threshold occurs later, allowing more emissions to accumulate.

~~At the same warming level, higher CO<sub>2</sub> concentration scenarios have a lower combined ocean and land carbon allocation fraction of the total carbon than lower CO<sub>2</sub> concentration scenarios.~~ These results are important for carbon budgets and mitigation strategies as they impact how much carbon the ocean and land surface could absorb [at a given warming level](#). Carbon budgeting will be key for reducing the impacts of anthropogenic climate change, and these findings could have critical consequences for policies aimed at reaching net zero.

**Keywords:** Climate change, ~~CMIP6, Earth System Models,~~ Carbon Cycle, Carbon Allocation, [CMIP6, Earth System Models](#)

## 1 Introduction

20 The Intergovernmental Panel on Climate Change (IPCC) Sixth Assessment Report ~~reported~~found that the global mean surface air temperature was 1.1°C warmer in the recent decade (2011-2020) than in the pre-industrial era. They found that human activities have indisputably caused this warming (IPCC, 2021b), with anthropogenic greenhouse gases, particularly carbon dioxide (CO<sub>2</sub>), being the primary cause.

Since the advent of the industrial revolution, carbon has been transferred gradually from fossil fuel reservoirs to the at-  
25 mosphere, primarily via combustion. Once in the atmosphere, some of the CO<sub>2</sub> is absorbed by the ocean via gas transfer, some is absorbed by the land surface via terrestrial carbon fixation, while some CO<sub>2</sub> remains in the atmosphere, as illustrated in figFig. 1. While these fluxes also occur naturally, the additional anthropogenic carbon load has perturbed the Earth ~~system~~System from its pre-industrial equilibrium. In the atmosphere, anthropogenic carbon causes additional warming (Hansen et al., 1981). In the ocean, anthropogenic carbon can cause acidification (Caldeira and Wickett, 2003) or participate  
30 in primary production or sequestration (Schlunegger et al., 2019). On the land surface, carbon can allow enhanced primary production and subsequent carbon sequestration. Once converted into biomass, this carbon may be a fuel source in fires (~~Burton et al., 2022; Sullivan et al., 2022~~). ~~Through its effect on transpiration rates, elevated atmospheric CO<sub>2</sub> can increase plant growth, impacting flood and drought risk (Ukkola et al., 2016), and which returns a portion of the sequestered carbon back to the atmosphere (Burton et al., 2022; Sullivan et al., 2022). Elevated atmospheric CO<sub>2</sub> can~~ worsen food quality and nu-  
35 trient concentrations (Erda et al., 2005)~~, and affect water-balance evapotranspiration, reducing streamflow in water-stressed regions (Ukkola et al., 2016).~~

The instantaneous distribution of anthropogenic carbon between the atmosphere, ocean and land surface is known as “carbon allocation in the Earth ~~system which we define as carbon allocation~~System” which we henceforth call “carbon allocation”. The balance between these carbon sinks is hugely important to climate projections and policymakers (IPCC, 2021b), impacting  
40 warming feedbacks, marine biogeochemistry and life on land (Macreadie et al., 2019; Hilmi et al., 2021). The physical and biogeochemical feedbacks could affect the future rates of greenhouse gas accumulation in the atmosphere, directly impacting warming (Canadell et al., 2021). They also directly influence the remaining carbon budget, which policymakers may use to limit fossil fuel consumption in order to keep warming in line with policy goals (Jiang et al., 2021). In addition, the balance of carbon between the atmosphere, land and ocean has large-scale consequences on the future of climate engineering via CO<sub>2</sub>  
45 removal and solar radiation modification (Lawrence et al., 2018). Changes to carbon allocation also impact several United Nations Development Programme Sustainable Development Goals, notably 13: Climate Action, 14: Life below Water and 15: Life on Land (United Nations, 2015).

In observations, the atmospheric CO<sub>2</sub> concentration is typically measured directly, while the ocean and terrestrial CO<sub>2</sub> sinks are estimated with global process models constrained by observations. For the decade 2008–2017, the Le Quéré et al. (2018)  
50 synopsis of ~~carbon cycle~~the global carbon budget summarised that the fossil fuel emissions were  $9.4 \pm 0.5$  PgC yr<sup>-1</sup>, and emissions from land use and land-use change was  $1.5 \pm 0.7$  PgC yr<sup>-1</sup>, most of which was due to deforestation. The growth of the atmospheric carbon was  $4.7 \pm 0.02$  PgC yr<sup>-1</sup>, the ocean carbon sink was  $2.4 \pm 0.5$  PgC yr<sup>-1</sup>, and the terrestrial carbon sink

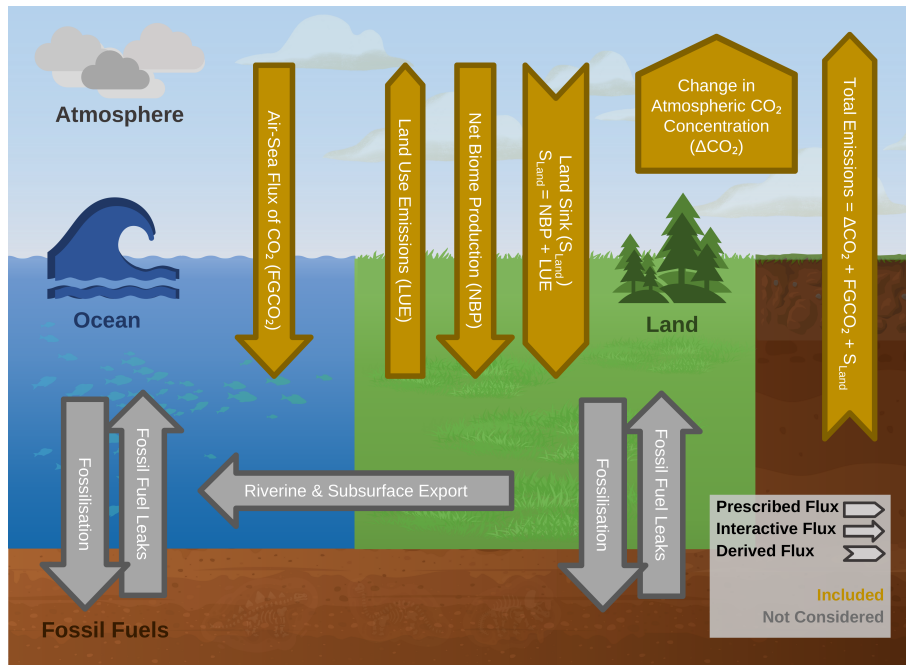


**Figure 1.** A simplified version of the Earth ~~system~~ System carbon cycle. Interactive fluxes are shown as arrows, prescribed fluxes are shown as box arrows, and derived fluxes are shown as chevrons. The arrows in gold are considered in this analysis, and the grey arrows are not considered. The prescribed change in atmospheric carbon,  $\Delta\text{CO}_2$ , accounts for the anthropogenic fossil fuel exploitation and the subsequent carbon emission. ~~Note that while in nature there is a flux of land carbon into the ocean via rivers, and there may be a flux of fossil fuels directly into the ocean or land surface via for instance fossil fuel extraction, these are not generally included in CMIP6 models.~~

was  $3.2 \pm 0.8 \text{ PgC yr}^{-1}$ . ~~In that synthesis, the~~ The difference between the estimated total emissions and the estimated changes in the atmosphere, ocean, and terrestrial biosphere was  $0.5 \text{ PgC yr}^{-1}$ , which indicated that there were either overestimated emissions or underestimated sinks or both. There is ~~a~~ also a flux of land carbon into the ocean via rivers between  $0.45 \pm 0.18 \text{ PgC yr}^{-1}$  and  $0.78 \pm 0.41 \text{ PgC yr}^{-1}$  (Jacobson et al., 2007; Resplandy et al., 2018; Hauck et al., 2020). ~~but this flux is not generally included in CMIP6 models (Jacobson et al., 2007; Resplandy et al., 2018; Hauck et al., 2020).~~ There may also be a direct flux of fossil ~~fuels directly~~ fuel extraction and other leaks into the ocean or land surface ~~via for instance fossil fuel extraction and other leaks~~ (Roser and Ritchie, 2023), but these are ~~not generally included in Earth system models.~~ also neglected in models.

It is ~~widely accepted that atmospheric CO<sub>2</sub> is correlated with the global mean atmospheric surface temperature.~~ Figure long established that the relationship between cumulative emissions and peak warming is insensitive to the emission pathway, either in the timing of emissions or the peak emission rate (Allen et al., 2009). More recently, figure 5.31 of Canadell et al. (2021) shows ~~also shows negligible pathway dependence between~~ the cumulative carbon emissions ~~against and the~~ global mean

65 temperature change ~~for in~~ several projections. ~~That figure shows a strong correspondence between emissions and warming which appears to be scenario independent.~~

The ~~warming climate and~~ rising atmospheric CO<sub>2</sub> ~~and warming climate~~ will cause major changes in vegetation structure and function over large fractions of the global land surface. ~~In Friend et al. (2014), an~~ An increase in global land vegetation carbon ~~was has been~~ projected, but with substantial variation between vegetation models (Friend et al., 2014). Much of the  
70 variability between ~~ESMs models~~ in global land vegetation carbon stocks was explained by differences in land vegetation carbon residence time (Jiang et al., 2015). In the ocean, the ~~mechanism is summarised by Katavouta and Williams (2021): an~~ increase in atmospheric CO<sub>2</sub> enhances the ocean carbon storage while warming acts to decrease the ocean carbon storage : (Katavouta and Williams, 2021).

Both the ocean and land carbon sinks are projected to continue to grow as the atmospheric concentration of CO<sub>2</sub> rises  
75 (Canadell et al., 2021). However, the combined fraction of emissions taken up by the land and ocean is projected to decline, and a larger fraction of the emissions will remain in the atmosphere. The carbon allocation at the year 2100 is strongly scenario dependent (IPCC, 2021a, fig. SPM7). ~~For instance, in SSP1-1.9, 30% of the carbon remains in the atmosphere in the (IPCC, 2021a, Fig. SPM7). The projected atmospheric carbon allocation in the year 2100 ,but in SSP5-8.5, that value is ranges from 30% in SSP1-1.9 to 62% -in SSP5-8.5. The Shared Socioeconomic Pathways (SSPs) are described below in sec. 1.1.~~  
80 While the land and ocean carbon uptake are expected to remain approximately equal, the uncertainty is much larger for the land carbon sink than the ocean. ~~In the land , some of the uncertainty~~ The uncertainty in the land sink is due to the balance of ~~increased land~~ carbon accumulation in the high latitudes ~~and against the~~ loss of land carbon in the tropics (Canadell et al., 2021) ~~-Further uncertainty arises from , and~~ the challenges of forecasting the water cycle, ~~including droughts that reduce especially droughts, which significantly reduce the~~ carbon absorption potential of the land surface (Ukkola et al., 2016; van der Molen et al., 2011; Ca  
85 . On the other hand, ~~the ocean CO<sub>2</sub> sink is strongly dependent on the emissions scenario. This continuous~~ absorption of carbon into the ocean reduces the mean global buffering capacity and drives changes in the global ocean's carbonate chemistry (Jiang et al., 2019; Katavouta and Williams, 2021). ~~These projections are based on data from the Coupled Model Inter-comparison Project (CMIP), and the most recent CMIP round, CMIP6, is described in sec. ?? , building a strong dependency on the choice of scenarios (Jiang et al., 2019; Katavouta and Williams, 2021).~~

## 90 1.1 Sixth Coupled Model Inter-comparison Project (CMIP6)

### 1.2 ~~Sixth Coupled Model Inter-comparison Project (CMIP6)~~

Earth System models (ESMs) are ~~one of the main tools to study the climatic impact of the combustion of fossil fuels, and they are the the~~ only tools capable of projecting ~~the a~~ future coupled carbon-climate system. The Sixth Coupled Model Inter-comparison Project (CMIP6) (Eyring et al., 2016) is the most recent ~~in a series of global efforts~~ global effort to stan-  
95 dardise, share and study ESM simulations ~~-To (Eyring et al., 2016). The CMIP6 standard simulation protocols, called the Diagnostic, Evaluation and Characterization of Klima (The DECK), are required simulations for a model to participate in CMIP6, models must meet certain model quality and data standards. These quality requirements include a drift. The DECK~~

includes a pre-industrial control, at least one historical simulation, a gradual 1% CO<sub>2</sub> growth experiment and a rapid 4xCO<sub>2</sub> experiment. For quality assurance, only models with a global drift per century lower than 10 PgC in the air-sea flux of CO<sub>2</sub> of less than 10 PgC per century, and a drift in the global flux and lower than 0.1 °C in the volume mean ocean temperature of less than 0.1 degrees per century are accepted (Jones et al., 2011; Eyring et al., 2016; Yool et al., 2020).

In order to make projections of the future anthropogenic climate drivers, multiple scenarios were proposed in the ScenarioMIP project to cover a wide range of potential futures (O'Neill et al., 2016). ScenarioMIP expands upon the CMIP6 core simulations and multiple scenarios are available for modellers to use to generate simulations (O'Neill et al., 2016). We include the scenarios: SSP1-1.9, SSP1-2.6, SSP2-4.5, SSP3-7.0 and SSP5-8.5 (O'Neill et al., 2016; Riahi et al., 2017) with multiple scenarios of the future anthropogenic climate drivers that cover a wide range of potential future climate and human behaviours (O'Neill et al., 2016). Scenario names in CMIP6 are comprised of a general future correspond with one of the five shared socioeconomic pathway (SSP1-SSP5) followed by an estimate of the radiative forcing at the year 2100 in units of between 1.9 and 8.5 Wm<sup>-2</sup>. These scenarios cover a wide range of possible futures, including sustainable development in the SSP1-5 are narratives that describe broad socioeconomic trends that are expected to shape the future of humanity, and are based on trends in population, urbanisation, and technological and economic growth (Riahi et al., 2017). In this work, we include: two sustainable development scenarios SSP1-1.9 and SSP1-2.6 scenarios. The “middle of the road” pathway in; the intermediate emissions scenario, SSP2-4.5 extrapolates historic and current global development into the future with, which has a medium radiative forcing by the end of the century. The; the regional rivalry scenario, SSP3-7.0, revives nationalism and regional conflicts, pushing which pushes global issues into the background and resulting in higher emissions. Then finally,; and the enhanced fossil fuel development in, SSP5-8.5 is a scenario with the highest feasible, which has extremely high fossil fuel deployment and atmospheric CO<sub>2</sub> concentration (Riahi et al., 2017) (O'Neill et al., 2016; Riahi et al., 2017).

## 1.2 Climate Sensitivity

Given the same rise in atmospheric CO<sub>2</sub> concentration, each ESM will warm by a different amount to a different temperature due to the significant structural and parametric differences between models. The Equilibrium Climate Sensitivity (ECS) is a measure of this sensitivity to CO<sub>2</sub>. The ECS is given in Celsius and represents the long-term defined as the global mean near-surface air temperature rise that is expected to result from in °C in response to a doubling of the atmospheric CO<sub>2</sub> concentration once the model has reached equilibrium. In effect, the ECS is an indicator for how much warming occurs in a model with a doubling of CO<sub>2</sub>. The most recent The 5-95% assessed natural ECS range was confidence range of ECS is between 2 °C and 5 °C, the likely ECS range was is 2.5 - 4 °C, and the most likely value was is 3 °C (Arias et al., 2021, TS6).

The wide spread of ECS values in climate (Arias et al., 2021, TS6). In ESMs, the spread in the sensitivity to CO<sub>2</sub> between models is one of the causes of uncertainty for in the timing of when forecasts projections reach certain warming levels. The Similarly, the uncertainty in the “allowable emissions” that would keep global temperature rise within policy targets are equally also impacted (United Nations Treaty Collection, 2015). This has been exacerbated in the latest round of CMIP, as the uncertainty is exacerbated in CMIP6 generation of ESMs as it has a broader range of sensitivities ECS values than previous generations. Several and several CMIP6 models have a stronger response to atmospheric carbon than any CMIP5 model, and

~~many sit above~~ are outside the likely ECS range (Arias et al., 2021, TS6). (Hausfather et al., 2022). Uncertainties in cloud feedbacks have been identified as the main cause of the large ECS range in CMIP6 (Ceppi and Nowack, 2021).

### 1.3 Global Warming Levels

135 Climate change policy ~~can often~~ has a tendency to focus on the climate at specific target years, ~~like such as~~ 2050 or 2100 (United Nations Treaty Collection, 2015; IPCC, 2021a). However, due to the wide range diversity of ECS values in ESMs, ~~this can mean that ensembles at the year 2100 are composed of a set of models with significantly different behaviours. This wide range in the temperatures and warming rates~~ CMIP6, the ensemble will project a wide range of warming rates and surface temperatures at a given point in time. This wide range of behaviours has knock-on effects on climate feedbacks and may inhibit the realism and ~~representativity~~ representativeness of the ensemble's multi-model mean (Hausfather et al., 2022; Swaminathan et al., 2022). On the other hand, this more comprehensive range of responses is valuable in exploring carbon-climate processes that are of direct relevance to policy. Instead of specific target years, we ~~can alternatively focus on model behaviour at focus on~~ three specific Global Warming Levels (GWL), ~~such as~~. These are 2 °C, 3 °C or 4 °C of warming relative to the pre-industrial period. ~~By investigating the system's behaviour at specific warming levels instead of target years, we can account for the impact of climate sensitivity and make~~ They allow us to generate policy relevant assessments while ~~still~~ exploiting the full ensemble of CMIP6 models. ~~This allows us to maintain model democracy, even in a so-called "hot model" ensemble.~~

~~The~~ Not only does the GWL methodology mirror the policy discourse surrounding the policy targets, it is also largely independent of the choice of future emissions scenario as the world largely looks the same at 2, 3 and 4 °C, no matter how we get there (Hausfather et al., 2022). In addition, GWL bypasses the need to select or weight CMIP6 models as each model provides distinct and relevant information, so the full CMIP6 ensemble can be used (Hausfather et al., 2022). The three GWLs were chosen because the 2 °C GWL is a key target set in the 2015 Paris Agreement (United Nations Treaty Collection, 2015) and thought to be a threshold for potentially dangerous climate change (United Nations Treaty Collection, 2015). The 3 °C GWL is the warming level that current nationally determined emission policies will realise for the year 2100 assuming a median climate sensitivity (United Nations Environment Programme, 2019). Finally, the 4 °C GWL is a low likelihood but high impact outcome if climate sensitivity is higher than median values or emission reductions and climate policy break down (World Bank, 2012).

This is the first work that presents the carbon allocation using ~~this the~~ the GWL framework. Previous analyses project carbon allocation at an arbitrary point in time using the mean of a set of models with widely different warming rates and sensitivities (IPCC, 2021a; Canadell et al., 2021). When compared against projections at specific points in time, our results are less influenced by the overall climate sensitivity of the ensemble and may be more relevant to policymakers.

## 2 Methods

### 2.1 Carbon allocation calculation

We calculate the carbon allocation for the land, ocean and atmospheric reservoirs separately. ~~On the land surface, the land~~ The land carbon sink,  $S_{Land}$ , is derived from ~~the global total~~ two other fields: the net biome production ( $NBP$ ) and the,  $NBP$ , and ~~global total land use emissions ( $LUE$ ). As  $NBP$  is defined as the difference between land sink and emissions from land use~~ ( $NBP = S_{Land} - LUE$ ), then:-

$$S_{Land} = NBP + LUE$$

~~The  $NBP$  is an prognostic~~,  $LUE$ . The  $NBP$  is a diagnostic variable calculated by the models and it is defined as positive for fluxes into the land carbon store in CMIP6 (Jones et al., 2016). ~~We calculated the~~  $S_{Land}$  is the activity of the vegetation, which is the combined carbon flux of all natural sources, including photosynthesis, respiration, wildfire and other sinks and sources. These natural fluxes and therefore the carbon sinks are altered by anthropogenic carbon emissions into the atmosphere, for example from fossil fuel combustion.  $S_{Land}$  is positive in the direction of a sink into the land from the atmosphere, but it does not the effects of anthropogenic land-use change. The  $LUE$  are anthropogenic carbon sinks and sources, including deforestation, land management, reforestation and others (Lawrence et al., 2016).  $LUE$  is positive into the atmosphere.  $NBP$  is a diagnostic that combines both  $S_{Land}$  and  $LUE$ .  $NBP$  is positive into the land, so for these sign conventions,  $NBP = S_{Land} - LUE$ , and represents the net exchange between land and atmosphere including anthropogenic emissions relating to land use change. The directions for these fluxes that are taken as positive are indicated in Fig. 1. To diagnose only the  $S_{Land}$  component, it is therefore necessary to add back in the  $LUE$  to  $NBP$ . As such,  $S_{Land}$  is here computed as the sum of the global total net biome production ~~as the cumulative sum over the entire global land surface of the  $NBP$  multiplied by the cell surface area.~~ From CMIP6 simulations, it and the global total land use emissions;

$$S_{Land} = NBP + LUE \tag{1}$$

ESMs produce  $NBP$  as a diagnostic field in the  $nbp$  dataset, but this is actually their total carbon change in the land. It is not possible to directly isolate the  ~~$LUE$  and so these are taken from~~  $LUE$  for each model and ensemble member in CMIP6 simulations, and the  $LUE$  value are calculated from prescribed land use scenarios and are common across all models and all ensemble members following Liddicoat et al. (2021). ~~As described in Pongratz et al. (2014) and Liddicoat et al. (2021), a~~ A more accurate method of determining the  ~~$LUE$  is~~  $LUE$  would be to calculate the difference in net biosphere production between a pair of simulations, one with land use changing over time, and the other with fixed land use (Pongratz et al., 2014; Liddicoat et al., 2021). However, these simulation pairs exist only for a limited subset of models and scenarios. ~~CMIP6 experiments express the  $LUE$  in units positive into the atmosphere, which is the opposite direction of the carbon flux in  $NBP$ .~~ as part of the Land Use Model Inter-comparison Project, LUMIP (Lawrence et al., 2016). In practice, we calculated the global total net biome production as the cumulative sum along the time axis of the land surface  $NBP$  multiplied by the cell surface area then summed with the annual  $LUE$  value from Liddicoat et al. (2021).

The ocean component of the carbon allocation,  $S_{Ocean}$ , is the total global sum of the air sea flux of  $CO_2$ . We calculated this as the sum of the air-sea flux of  $CO_2$  multiplied by the ocean area of each cell, expressed as a cumulative sum of the annual  
195 totals. Like the land surface, the ocean can be both a sink and a source of  $CO_2$ .

In the atmosphere, the global mean  $CO_2$  concentration is provided in the scenario forcing from ScenarioMIP in units of parts per million (ppm). The total mass of the carbon in atmospheric  $CO_2$ ,  $C_{Atmos}$ , is calculated by multiplying the change in concentration relative to the 1850 value in ppm by a constant factor. This conversion factor is +ppm-of-2.13 PgC per ppm change in  $CO_2$  is equivalent to 2.13 PgC concentration (Myers, 1983). No matter how much carbon the land and ocean  
200 components absorb from the atmosphere, the atmospheric concentration of  $CO_2$  will always strictly follow the prescribed atmospheric  $CO_2$  concentrations of the forcing scenario. This means that anthropogenic emissions can be estimated for each model (Jones et al., 2013). The total anthropogenic carbon,  $C_{Total}$ , is the sum of the total carbon in the atmospheric  $CO_2$ ,  $C_{Atmos}$  and the cumulative global total  $CO_2$  flux into the sea and the true land sink,  $S_{Ocean}$ , and the land sink,  $S_{Land}$ :

$$C_{Total} = C_{Atmos} + S_{Ocean} + S_{Land} \quad (2)$$

## 205 2.2 Included Models

This analysis used all CMIP6 ESMs for which the following three variables were available as monthly averages over the time period 1850-2100: the near-surface atmospheric temperature (~~tast~~), the net biome productivity (~~nbp~~) and the air to sea flux of  $CO_2$  (~~fgeo2fgco2~~). We limited each model to only the first ten ensemble members for each scenario, and required at least one historical and future scenario pair for each ensemble member. The grid cell area was also required for the ocean  
210 (~~areacellareacello~~), and for land and atmosphere (~~areacellaareacella~~) grids. We excluded the entire ensemble member if any variables were absent, the time series was incomplete, or the data could not be made compliant with CMIP6 standards.

In CMIP6, modelling centres may contribute more than one ensemble member for each scenario to the Earth System Grid Federation (ESGF). For instance, the UKESM1-UKESM1-0-LL model produced 19 different variants for the historical experiment, each using slightly different initial conditions drawn from the pre-industrial control (piControl) simulation (Sellar et al.,  
215 2020). This generates an ensemble of variants which samples a wide range of the unforced variability simulated by the model. By spanning the range of internal variability simulated by the model, the mean of a single model ensemble can give a more robust estimate of the-its forced climate change -response.

Each modelling centre may-choose-has flexibility on which scenarios they simulate and how many ensemble members are generated for each scenario. This means that there is wide variation in the number of ensemble members between models.  
220 To balance models with large ensembles against models with small ensembles, we used a “one model - one vote” weighting scheme. This ensured that each model was given equal weight in the final multi-model mean. In practice, each ensemble member of a given model was weighted inverse-proportionally-inversely proportional to the number of ensemble members that the model contributed. No effort was made to weigh For reasons described in Sect. 1.3, we did not weigh the results regarding the model quality, sensitivity or historical performance.

225 Table 1 lists the contributing models, the number of ensemble members for each scenario, and each model’s equilibrium climate sensitivity (ECS). The ECS plays a first order role in how rapidly a given model reaches a given GWL for a given  $CO_2$



pathway. For most models, we took the ECS value from Zelinka et al. (2020). For the models whose ECS was not included in Zelinka et al. (2020), we use the following ECS values: ACCESS-ESM1-5 from Ziehn et al. (2020), CMCC-ESM2 from Lovato et al. (2022), EC-Earth3-CC from Hausfather et al. (2022), GFDL-ESM4 from Dunne et al. (2020), and MPI-ESM1-2-LR from Mauritsen et al. (2019). No ECS value was available for the CanESM5-CanOE model as it did not provide the abrupt 4xCO<sub>2</sub> experiment required to calculate ECS using the Gregory method (Gregory et al., 2004; Christian et al., 2022). However, it only differs from CanESM5 by the addition of a marine ~~BGC-biogeochemistry~~ component model (Swart et al., 2019; Christian et al., 2022). We follow the method used elsewhere (Hausfather et al., 2022; Scafetta, 2022), and substitute CanESM5's ECS value for CanESM5-CanOE. Other ECS datasets also exist, see for instance: Flynn and Mauritsen (2020); Meehl et al. (2020); Weijer et al. (2020); Hausfather et al. (2022), and only ~~have small differences in their values~~ differ within 0.1 °C from the values used in this study. All ECS values included here use the Gregory et al. (2004) method, however, the value of ECS for any given model is sensitive to the method that was used to derive it. See for instance ~~tab. Table~~ Table 4 of Boucher et al. (2020), where ECS for the same model ~~varies may vary~~ by more than ~~a degree~~ 1 °C depending on the methodology.

~~This table also~~ In its last row, Table 1 shows the ensemble mean ECS of the contributing models for each scenario ~~in the last row. The weighted ECS is only weighted by~~ Following the “one-model one-vote” scheme, the “weighted ECS” only takes into account the presence or absence of models, not the number of contributing ensemble members, ~~reflecting the “one-model one-vote” weighting scheme described above~~. The spread of weighted ECS values between scenarios is small, ranging from 3.96 for SSP1-1.9 to 4.17 for SSP5-8.5. Five out of six of these ensemble means sit above the likely ECS range of 2.5 ~~°C~~ - 4 °C, and four of the individual models are outside the 5-95% confidence band, ~~2 °C and~~ 5 °C (Sherwood et al., 2020; Arias et al., 2021).

As in other CMIP ensemble studies, we attempt to maximise the number of models in this work (~~Flynn and Mauritsen, 2020; Meehl et al.~~ so in order to improve robustness (Flynn and Mauritsen, 2020; Meehl et al., 2020; Weijer et al., 2020; Hausfather et al., 2022) This means that we allow all available candidates, even pairs of sibling models: there are two CESM2 models and two CanESM5 models in the ensemble. CESM2-WACCM6 is configured identically to CESM2, except that it has expanded aerosol chemistry and uses 70 vertical levels and its model top is at  $4.5 \times 10^{-6}$  hPa (approximately 130 km), instead of CESM2's 32 vertical levels and a model top at 2.26 hPa (approximately 40 km) (Danabasoglu et al., 2020). The CanESM5-CanOE model differs from CanESM5 by the addition of a more complex marine biogeochemistry component (Christian et al., 2022).

In addition to sibling models, the same individual component models are used by several modelling centres. For instance, the NEMO ocean circulation model forms the marine circulation component model of six of the ~~earth system models~~ ESMs used here (Heuzé, 2021). While the ESMs use differing versions of NEMO with different configurations and settings, these models can not be treated as statistically independent. However, it is beyond the scope of this work to develop or apply a method to weight models such that the multi-model mean is statistically robust, for instance in Brunner et al. (2020).

### 2.3 Global warming level calculation

We calculated the global warming level following the methods of Swaminathan et al. (2022). The global mean atmospheric surface temperature is calculated for each model, scenario and ensemble member. The anomaly is the difference from the

**Table 1.** A list of the models, the number of contributing ensemble members for each scenario, the model ECS, and the weighted mean ECS of the contributing models. The weighted ECS row shows how the model occupancy affects the mean ECS of the ensemble for each scenario. The presence or absence of models impacts the weighted ECS, but not the number of contributing ensemble members.

Model	Historical	SSP1-1.9	SSP1-2.6	SSP2-4.5	SSP3-7.0	SSP5-8.5	ECS
ACCESS-ESM1-5	3		2	3	2	1	3.87
CESM2	3		3	3	3	3	5.15
CESM2-WACCM	3		1	3	1	3	4.68
CMCC-ESM2	1			1			3.57
CanESM5	10	10	10	10	10	10	5.64
CanESM5-CanOE	2		2	2	2		5.64
EC-Earth3-CC	8			8		1	4.23
GFDL-ESM4	1	1	1	1	1	1	2.7
IPSL-CM6A-LR	12	5	3	6	10	5	4.56
MIROC-ES2L	5	5	5	5	5	5	2.66
MPI-ESM1-2-LR	5	5	5	5	5	5	2.83
NorESM2-LM	2		1	2	1		2.56
UKESM1-0-LL	10	5	10	10	10	5	5.36
Total number of Ensembles	65	31	43	59	50	39	
Total number of Models	13	6	11	13	11	10	
Weighted ECS	4.11	3.96	4.15	4.11	4.15	4.17	

mean of the period 1850-1900 from the relevant historical ensemble member. This temperature time series is then smoothed by taking the mean of a window with a width of 21 years, i.e. 10 years either side of the central year. The first year that the smoothed global mean surface temperature anomaly exceeds the global warming level is the GWL exceedance year (see Fig. 1 of Swaminathan et al. (2022)). ~~Note that due~~ Due to the 21 year window and simulations ending in 2100, the last possible  
265 GWL exceedance year is 2090.

We calculate the multi-model mean for each of the variables using the “one model - one vote” scheme described above. We also determine the multi-model mean GWLs and their timings from the multi-model mean temperature, instead of taking the weighted mean of the individual ensemble members GWLs timings. This method ensures that the multi-model mean is more representative of the overall ensemble, instead of being biased towards only those models that reach the GWL.

270 We used the ESMValTool toolkit to perform the analysis. ESMValTool is ~~a software toolkit that was~~ built to facilitate the evaluation and inter-comparison of CMIP datasets by providing a set of modular and flexible tools (Righi et al., 2020). These tools include quick ways to standardise, slice, re-grid, and apply statistical operators to datasets. In our case, we used the `annual_statistics` preprocessor to calculate the annual mean, the `mask_landsea` preprocessor to mask the land or

ocean areas, and the `area_statistics` preprocessor to calculate the area weighted global mean. ESMValTool is hosted on  
275 GitHub and aH, and we have made available all of the code used in the [code we used here is available as described in the study](#)  
([see Code and data availability section](#)).

### 3 Results

#### 3.1 Multi-model mean carbon allocation

The total multi-model mean carbon allocation for each scenario at the year 2100 and for each of the three warming levels (GWLs)  
280 is shown in [fig Fig. 2](#). The left side shows the percentage allocation, and the right side shows the totals in PgC. In the top panes  
showing the [The top pane shows the](#) carbon allocation at the year 2100. At 2100, the higher emission scenarios have greater  
total carbon allocations with and more of that carbon is allocated to the atmosphere, relative to the lower emission scenarios.  
At the year 2100, more carbon is [allocation allocated](#) to the ocean than the land in SSP5-8.5, SSP3-7.0 and SSP2-4.5, while  
more carbon is [allocation allocated](#) to the land than the ocean in [SSP1-2.6](#), SSP1-1.9 and [SSP1-2.6](#). This reproduces the results  
285 discussed earlier from [\(IPCC, 2021b, fig. SPM7\)](#). [IPCC \(2021b\) Fig. SPM7](#).

The lower three [rows of this figure panes of Fig. 2](#) show the carbon allocation at each GWL. In all cases, the variability  
between scenarios within a single GWL is significantly less [that than](#) the variability between scenarios at the year 2100 in the  
top pane. However, the variability within the same GWL is still significant in absolute terms. For instance, the multi-model  
mean [total carbon allocation for the](#) 2 °C GWL ranges from 909 PgC in SSP2-4.5 to 972 PgC in SSP3-7.0 (a range of 63 PgC).  
290 At the 3 °C GWL, the range is 56 PgC and at 4 °C GWL, the range is 15 PgC. When compared against the annual total  
emissions estimate,  $9.4 \pm 0.5 \text{ PgC yr}^{-1}$  (Le Quéré et al., 2018), these differences between scenarios represent several years'  
worth of the global total anthropogenic emissions.

In the land surface, the multi-model [mean 2 °C GWL has means have](#) a range of 46 PgC, 35 PgC [at the 3 °C GWL](#), and 52 PgC [between](#)  
[scenarios for the 2 °C GWL, and at 4 °C GWL, the range is 52 PgC between scenarios, 4 °C GWLs respectively](#). The recent  
295 annual terrestrial carbon sink was  $3.2 \pm 0.8 \text{ PgC yr}^{-1}$  (Le Quéré et al., 2018), so the difference between scenarios is equivalent  
to at least a decade's worth of current carbon absorption by the land surface.

[In the ocean, the 2 °C GWL carbon allocation has](#) [The multi-model means of the ocean flux have](#) a range of 28 PgC, [the](#)  
[3 °C GWL has a range of](#) 34 PgC, and [at 4 °C GWL has a range of](#) 21 PgC between scenarios [for the 2 °C, 3 °C, 4 °C GWLs](#)  
[respectively](#). This reflects the previous result that the carbon allocation to the land surface is more variable than the ocean,  
300 as the land values have [a wider range wider ranges](#). The recent annual ocean carbon sink was  $2.4 \pm 0.5 \text{ PgC yr}^{-1}$  (Le Quéré  
et al., 2018). Similarly to the land case described above, the difference between scenarios is equivalent to approximately [a one](#)  
decade worth of [the](#) current ocean carbon absorption.

In the left hand side of [fig Fig. 2](#), the higher CO<sub>2</sub> concentration scenarios have a larger atmospheric fraction than lower CO<sub>2</sub>  
concentration scenarios at the same GWL. For instance, the atmospheric fraction is 46% in SSP5-8.5 and 42% SSP1-2.6 at the  
305 2 °C GWL, and the atmospheric fraction is 51.2% in SSP5-8.5 and 47.4% SSP2-4.5 at the 3 °C GWL.

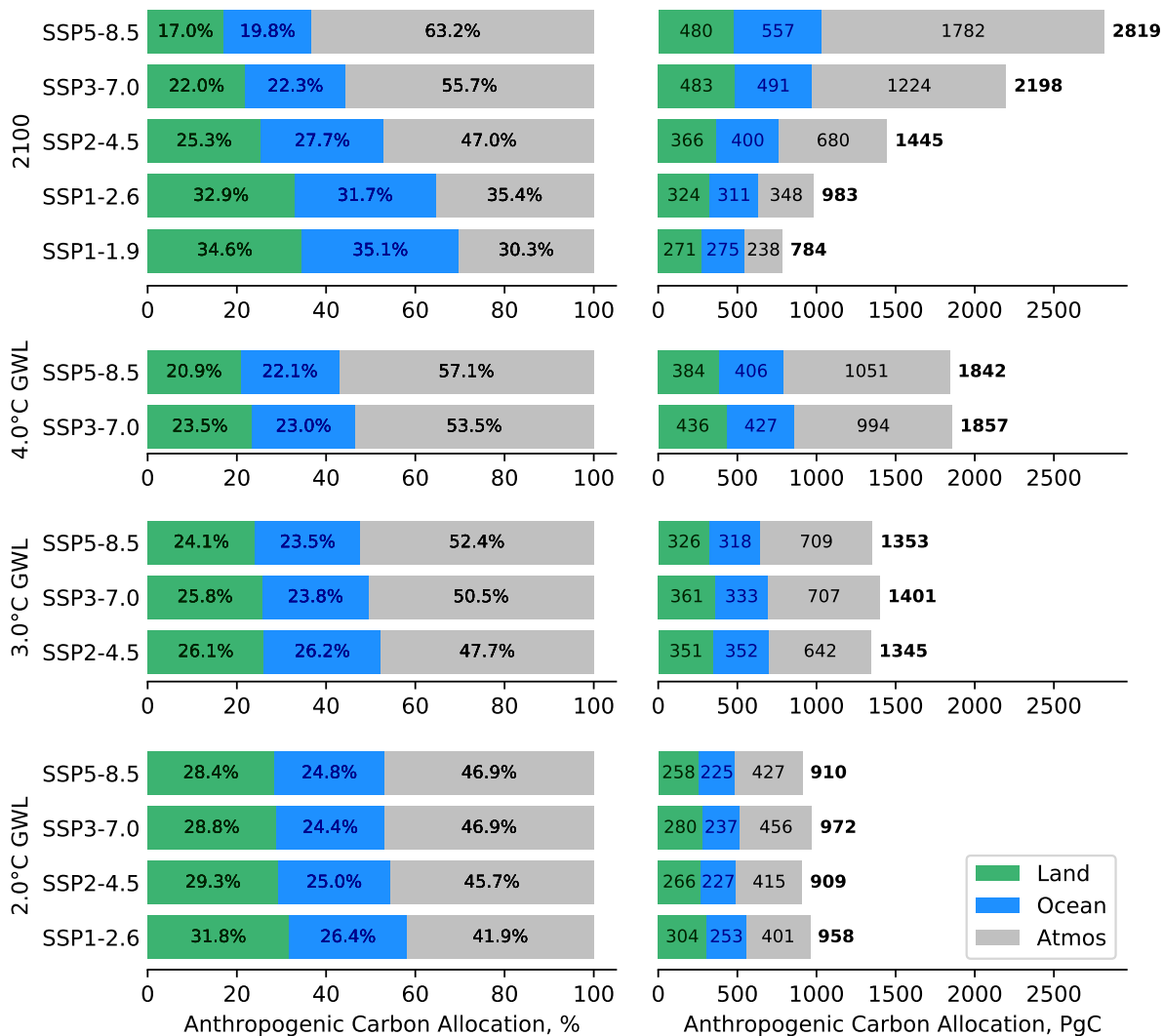


**Figure 2.** Carbon allocation for the multi-model mean for each scenario for the year 2100 and the three GWLs. The green, blue and grey areas represent the land, ocean and atmospheric carbon allocations. On the left hand-side, the x-axis shows the carbon allocation as a percentage allocation, and the right hand-side shows the cumulative total totals in PgC. The total values are shown in bold to the right of the bars. Note that these values are rounded to the nearest 0.1% or the nearest integer PgC, so the three values may not add exactly to 100% or the total.

Figure 2 only shows the multi-model means, not single models. This means that, so the multi-model means that do not reach the GWL are not included in this figure. Table 1 shows that there are six models contributing to the SSP1-1.9 scenario in this analysis, yet the multi-model mean does not reach the 2 °C GWL here. Similarly, there are 11 SSP1-2.6 models, but the

multi-model mean does not reach the 3 °C GWLs before the year 2100, nor does the mean of [the](#) 13 SSP2-4.5 models reach   
310 ~~the~~ 4 °C of warming.

### 3.2 Carbon allocation time series

The CMIP6 multi-model mean carbon allocation time series is shown in [figFig. 3](#). ~~This figure includes a pair of panes for each scenario. For each pair, the top pane is the cumulative carbon in PgC and the bottom pane shows the percentage. The sum of the three sinks estimates the total anthropogenic emissions. The~~ [The](#) top left pair shows the development over the historical   
315 period and the other five pairs show the ~~future scenarios~~[projections](#). We include all data cumulatively from the year 1850, and all the cumulative carbon panes share the same y-axis range. The timing of each of the multi-model mean GWLs are marked as vertical lines.

In the historical pane of [figFig. 3](#), the fractional atmospheric carbon starts to grow in the second half of the 20<sup>th</sup> century, as the land fraction declines and the ocean fraction increases. However, all three reservoirs increase in absolute terms over the   
320 entire historical period. By the end of the historical period, the land and ocean match the observational records of Raupach et al. (2014) and Watson et al. (2020) reasonably well, shown as dashed horizontal lines. In future scenarios, the [global warming level GWL](#) threshold year occurs sooner in higher concentration scenarios than in lower concentrations scenarios. In all scenarios, the total anthropogenic carbon rises until at least the year 2050. In the two SSP1 scenarios, the total carbon starts to fall after this point, while it continues to grow in the other projections.

325 The fraction of carbon that is absorbed by the combined land and ocean reservoirs rises in the two SSP1 scenarios, remains approximately constant in SSP2-4.5 after 2050, and declines in the SSP3-7.0 and SSP5-8.5 scenarios. The time series at the year 2100 closely match the IPCC atmospheric fraction projections for the year 2100 ([IPCC, 2021b, fig. SPM7](#)) ([IPCC, 2021b, Fig. SPM7](#)), shown in [figFig. 3](#) as a [short](#) horizontal line at the end of the period. This corroboration of existing results allows an increased confidence that our methodology is ~~correct~~[appropriate](#).

### 330 3.3 Multi-model ensemble carbon allocation

Figure 4 shows the carbon allocation at each GWL as a percentage ~~and the total value~~ [\(left\) and in terms of the total carbon](#)   
for each model [\(right\)](#). For each scenario and each GWL, the models are ordered by their ECS as shown in [tab:Table 1](#). The lower ECS models are at the top and higher ECS models ~~on are at~~ [the bottom](#) of each section. The lower sensitivity models take longer to reach the same warming level and have more total emissions than the higher sensitivity models. This results in   
335 the saw-tooth pattern on the right of this figure. ~~However, this saw-tooth pattern does not appear on the left side of the figure, as the ratios of carbon allocation between land, ocean and atmosphere at a given GWL are not dependent on ECS.~~

There is a significant variability between individual models in the total [carbon cumulative carbon allocated](#) between scenarios at each GWL. For instance, the total carbon [change](#) at 2 °C ranges from 615 PgC (CanESM5-CanOE, SSP3-7.0) to 1521 PgC (NorESM2-LM, SSP3-7.0). This range of behaviours between models is very large and the difference between these two extremes is equivalent to a century's worth of current global emissions, ~~(i.e. 100 years of  $9.4 \pm 0.5$  PgC yr<sup>-1</sup> Le Quéré et al. (2018))~~ [\(Le Quéré et al., 2018\)](#).

### Anthropogenic Carbon Allocation Timeseries

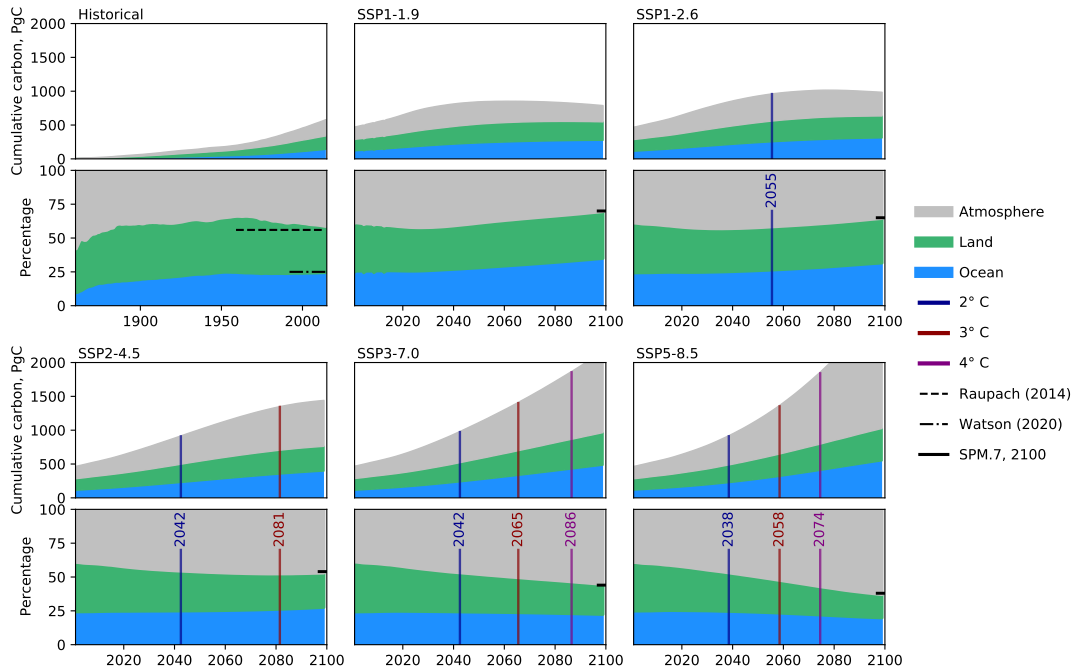


**Figure 3.** Multi-model mean carbon allocation time series for the historical period and each scenario. The Each scenario includes a pair of panes: the top pane of each pair shows the total allocation in PgC, and the bottom pane shows the allocation as a percentage. The historical pane includes the historical observations-observational records for the land and ocean fractions, from Raupach et al. (2014) & Watson et al. (2020), and the length of the lines represent the time over which the data was collected for these two observational datasets. The future pane shows the atmospheric fraction projection for 2100 from IPCC (2021b). The grey area is the cumulative anthropogenic carbon in the atmosphere, and the blue and green represent the fraction in the ocean and in the land, respectively. The SPM7 lines at the year 2100 indicate the atmospheric fraction projections from the IPCC AR6 WG1 summary for policymakers figure 7, IPCC (2021b).

Proportionally large ranges can also be seen in the land, ocean and atmospheric carbon sinks in figFig. 4. For instance, at the 2°C warming °C GWL, the land may have absorbed as little as has absorbed between 164 PgC (EC-Earth3-CC SSP2-4.5) or as much as and 432 PgC (MIROC-ES2L ,SSP3-7.0). Similarly, at at the 2°C warming °C GWL, the ocean may have 345 absorbed as little as has absorbed between 137 PgC (CanESM5-CanOE SSP3-7.0) or as much as and 401 PgC (NorESM2-LM SSP2-4.5). These ranges are equivalent to several decades worth of current global emissions, or approximately a century of the current annual rates of land or ocean carbon absorption. Almost all of the minimum and maximum values described here occur in the SSP3-7.0 scenario, for reasons described below in Sect. 4.2.

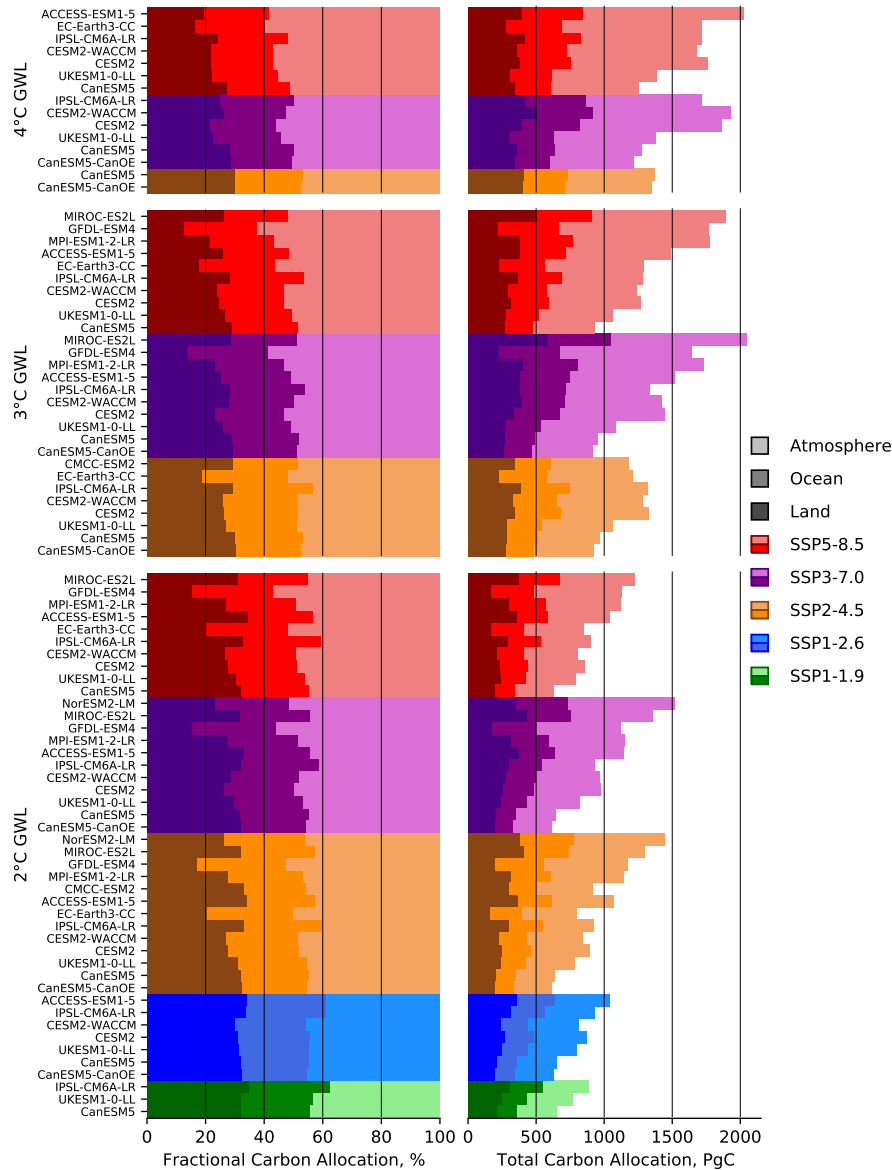


**Figure 4.** Global total carbon allocation for each level of warming for individual models. The left side shows the allocation as a percentage and the right side shows the total value in PgC. Each colour palette represents a different scenario, with SSP1-1.9 in greens, SSP1-2.6 in blues, SSP2-4.5 in oranges, SSP3-7.0 in purples and SSP5-8.5 in reds. The darkest shade denotes the land, the middle shade is the ocean and the lightest shade is the atmosphere. Within a given GWL and scenario, the models are ordered by their ECS, with less sensitive models at the top and more sensitive models at the bottom.

The left side of this figure shows several key results related to how carbon is allocated as a percentage of the total between 350 models. **Firstly, at a given GWL, higher emission scenarios have a higher atmospheric fraction. In effect, the SSP5-8.5**

scenarios have a higher atmospheric fraction than SSP1-1.9 and SSP1-2.6 scenarios, even at the same GWL. Similarly, higher emission scenarios have a smaller, a lower land fraction, while the ocean fraction is similar across scenarios at the same GWL. Secondly, warmer GWLs have a larger atmospheric fraction than cooler GWLs. Thirdly warmer GWLs have a smaller land fraction and a relatively consistent ocean fraction. Warmer GWLs have larger atmospheric fractions, lower land fractions, and consistent ocean fractions than cooler GWLs. Finally, the ocean fraction is relatively consistent between GWLs and scenarios.

### 3.4 Carbon allocation and ECS

The data from Fig. 4 is re-framed in Fig. 5 as a series of scatter plots. In this figure, each row represents a different scenario, and each column is a different dataset. These datasets are the GWL threshold year, the total carbon allocated, the carbon allocation for each domain and the fractional carbon allocation to each domain. The y-axis shows the model's ECS, and each point is a different GWL, where the squares are 2°C GWL, the circles are 3°C GWL, and the triangles are 4°C GWL. In all cases, the darkest colours are the 2°C GWL, the middle colour are the 3°C GWL, and the lightest colours are the 4°C GWL. For each group of data, the line of best fit is shown and the absolute value of the fitting error (Err) of the slope (M, the standard error of the estimated gradient under the assumption of residual normality) over the slope (M) is shown in the legend, as  $Err/M$ . The fitting error, Err, here is the standard error of the estimated gradient under the assumption of residual normality. This value indicates whether the slope crosses the origin within the 95% confidence limit. If the uncertainty on the slope is greater than the slope itself (and  $Err/M$  exceeds unity), then we can assume that the fit is not statistically significant. ( $Err/M < 1$ ) or not ( $Err/M > 1$ ). While the value always appears in the legend, the line of best fit is only shown when  $Err/M < 1$ . All groups with three models or fewer that reach the GWL were excluded as there were not enough data points to draw meaningful conclusions.

The goal of this figure is to highlight in broad strokes the ways that ECS interacts with carbon allocation in these models. GWL year, total carbon change and the individual total carbon allocation fractions are inversely correlated to ECS. The GWL threshold year and the total carbon allocations both have all  $Err/absolute\ Err/M$  values lower than unity and as such are both correlated with ECS. In both are related to ECS. The total carbon change in both the ocean and the atmosphere's total carbon, the absolute value of  $Err/M$  is always smaller than one. This means that the total carbon in both the ocean and the atmosphere is correlated with the ECS with 95% confidence. However, this is not the case for the ocean or the atmosphere's carbon allocation as a percentage and in many cases  $Err/M$  are linked to ECS, as their  $Err/M$  are smaller than 1. However, the correlations between carbon allocation fraction of the ocean or the atmosphere and ECS are not statistically significant. For land, both the total carbon sink and the allocation fraction are not consistently correlated to ECS at all GWLs.

In addition to the GWL data, the values for the target year 2100 are shown in Fig. 5. The  $Err/M$  for the target year 2100 is greater than unity. This means that we can not say that the fraction of carbon allocated to the ocean or to the atmosphere is correlated with the ECS with 95% confidence. Similarly, this  $Err/M$  ratio is not consistently below unity for the land ensembles at all GWLs. This implies that the total or percentage land carbon allocation is likely to be not correlated with ECS. In the total carbon, the atmospheric carbon fraction, and both land columns, indicating a poor fit to a straight line. This indicates that ECS is not correlated to these data in target year analysis. Elsewhere, when the  $Err/M$  of the target year 2100 is less than one, it



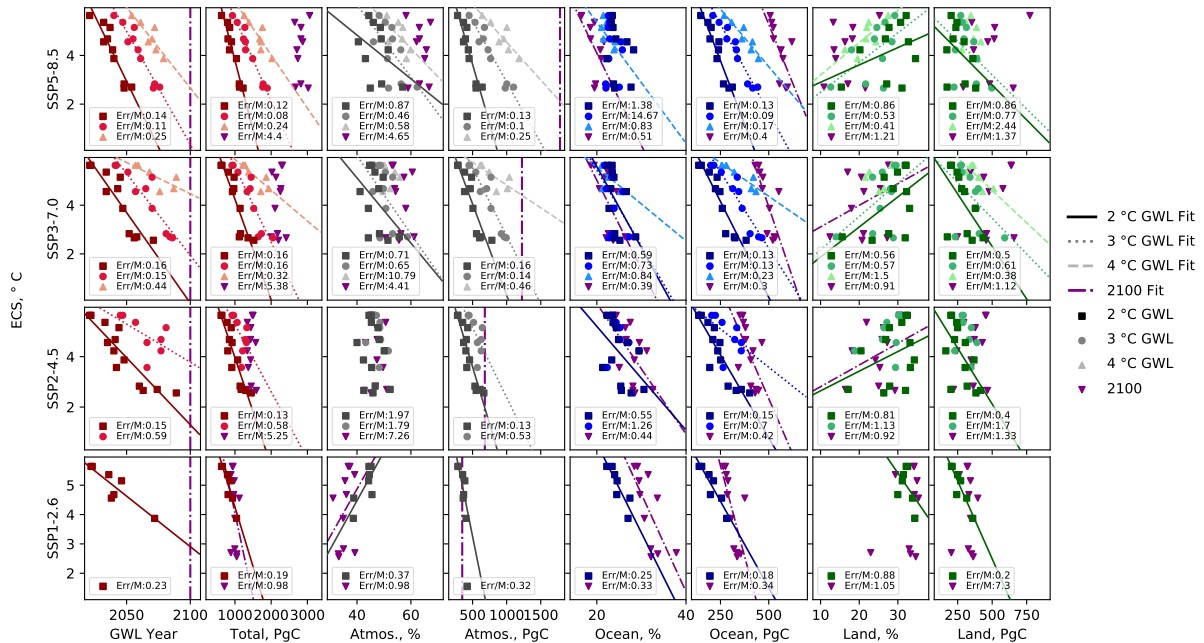


**Figure 5.** The GWL and target year 2100 carbon allocation scatter plot matrix for each. Each row represents a different scenario, and each column is a different data field, including the GWL-year, the total carbon allocated, the carbon allocation for each domain and the fractional carbon allocation to each domain. The y-axis is the model's ECS, and each point is a different GWL, where the squares are the 2° GWL, the circles are the 3° GWL, and the triangles are the 4° GWL. In all cases, the darkest colours is-correspond to the 2° GWL, the middle colour-are colours the 3° GWL, and the lightest colours are-the 4° GWL. For each group of data, The results for the line of best fit is target year 2100 are also shown and the in purple downward-pointing triangles. The absolute value of the fitting error of the slope over the slope is shown in the legend as Err/M. The line of best fit is shown when  $Err/M < 1$ . The year 2100 and the total atmospheric carbon are indicated with purple vertical dash-dot lines.

385 is often close to unity or larger than the Err/M of the fits to the GWL data. This indicates that ECS is often less correlated to these data in target year analysis than the GWL values. The GWL method allows us to characterise the impact of ECS, while the target year method obscures its influence.

#### 4 Discussion

390 We have shown-We present an analysis of the carbon allocation in the Earth System for an ensemble of CMIP6 simulations at three-the 2, 3 and 4 °C global warming levels. By-We find that through using the GWL method instead of focusing on a specific target year, we can provide estimates of the behaviour of the carbon cycle that may be more useful and relevant to policy-makers.-In figpolycymakers. In Fig. 2, the difference between a focus on a specific year and the GWL method can clearly be seen by comparing the top pane against the other three panes. At the year 2100, there are large differences between

the five scenarios total carbon change, the allocation between the three reservoirs and the fractional distribution. ~~However, it's~~  
395 ~~not possible to use this target year method to unpick where those differences between scenarios originate.~~ In the lower three  
panes, the differences between scenarios is much smaller. However, these small differences are still significant in absolute  
terms, where several years-worth-year's worth of global CO<sub>2</sub> emissions separate the scenarios at each GWL.

~~This method allows a closer analysis of~~ The pathway to a given GWL is scenario-dependent in two main ways. Firstly,  
the rate of anthropogenic CO<sub>2</sub> emissions has a non-negligible impact on the atmospheric fraction because the ocean and  
400 land surface can not quickly absorb the additional carbon load. A higher rate of emission leads to a slightly greater transient  
warming, because fractionally more of the emitted CO<sub>2</sub> is still in the atmosphere. Secondly, CO<sub>2</sub> is the primary but not the  
only driver of warming. Differences between the non-CO<sub>2</sub> forcings play a role in the realised warming at a given point in time  
in these scenarios. In addition, while the composition of each scenario ensemble results in a relatively uniform set of values of  
the mean ECS in Table 1, the mean ECS does vary by up to 0.21 °C between scenarios. This could also account for some of  
405 the differences seen between multi-model means in Fig. 2. Furthermore, the SSP1-1.9 ensemble has the lowest mean ECS and  
the SSP5-8.5 ensemble has the highest mean ECS, which may exaggerate the differences between their multi-model means.

The GWL methodology allows a focused analysis on the small and subtle differences between scenarios ~~seen in previous~~  
~~works.~~ For instance, ~~fig~~ in Canadell et al. (2021), Fig. 5.31 of Canadell et al. (2021) shows the cumulative carbon emissions  
against global mean temperature change for several projections. In that figure, all five projections show a strong correlation  
410 between CO<sub>2</sub> emissions and warming. ~~In addition,~~ all projections overlap at the same cumulative ~~carbon dioxide emissions~~  
~~. Due to results like these, it is widely thought that there are not significant differences in the carbon behaviour of these~~  
CO<sub>2</sub> emissions and there are no clear differences between scenarios for the same cumulative ~~carbon dioxide~~ CO<sub>2</sub>. Using the  
GWL method, we ~~have placed these results under the microscope and demonstrated that non-trivial~~ are able to focus on the  
differences between scenarios at the same warming level and demonstrate that small differences exist between scenarios and  
415 that the pathway to a GWL matters. ~~However, these differences are only for the carbon allocation. While these differences~~  
in carbon allocation may only be visible under the zoomed-in focus of a GWL analysis. ~~Our conclusions are compatible~~  
~~with previous works and we do not claim to refute the results of Canadell et al. (2021),~~ the differences between scenarios are  
consistent with previous studies and are likely due to differences in non-CO<sub>2</sub> forcing. However, it is beyond the scope of this  
work to quantify the non-CO<sub>2</sub> effect as in Smith et al. (2020).

420 On the left side of ~~fig~~ Fig. 2, the fraction of carbon that remains in the atmosphere is linked with the choice of scenario.  
The higher emission scenarios have higher atmospheric fractions (~~AF~~) at the same warming level. The ~~mechanism here is~~  
~~most likely to be~~ likely mechanism is that scenarios with higher carbon concentrations simply reach the global warming levels  
sooner, and have proportionally less carbon allocated to the ocean and land surface at that time. The ocean and the land ~~hasn't~~  
~~had time to catch~~ had not caught up with the emissions or the warming associated with that ~~carbon dioxide~~ CO<sub>2</sub> concentration.  
425 This implies that the carbon allocation between the three major sinks is likely impacted by the rate of warming at the GWL  
and there may be some delay between ~~emissions and carbon allocation~~ CO<sub>2</sub> emissions and the equilibrium CO<sub>2</sub> atmospheric  
fraction, as the excess CO<sub>2</sub> is slowly absorbed by the terrestrial and oceanic sinks.

In the land surface at the 4 °C GWL, the multi-model mean land vegetation carbon increases by 384 and 436 PgC relative to 1850 in SSP5-8.5 and SSP3-7.0 respectively, as shown in [fig Fig. 2](#). In [Friend et al. \(2014\) CMIP5](#), the range relative to the years 1971-1999 was 52–477 PgC with a mean of 224 PgC, and was attributed mainly due to CO<sub>2</sub> fertilisation of photosynthesis ([Friend et al., 2014](#)). While our CMIP6 multi-model mean is compatible with Friend et al. (2014)'s CMIP5 result, we do not see any individual model with only 52 PgC carbon allocated to the land at the 4 °C GWL in [fig 4](#). This absence is more likely to be attributed to the difference in the anomaly period (1850 vs 1971), rather than due to the significant changes between CMIP5 and CMIP6 land surface models. [The VISIT is the land component](#) model that contributed [the minimum value of 52 PgC in Friend et al. \(2014\) PgC in Friend's](#) CMIP5 analysis, [VISIT, and VISIT](#) is part of the MIROC-ES2L ESM in CMIP6 ([Hajima et al., 2020](#)). However, MIROC-ES2L did not reach the 4 °C GWL in any scenario presented here. In all aspects of this analysis, the land carbon allocation has a much wider range of variability than the ocean. This reflects the significant challenge and uncertainty inherent in modelling the land surface carbon cycle ([Friend et al., 2014; Jiang et al., 2019](#)).

When comparing the same model at the same GWL between scenarios, the differences between scenarios becomes even more apparent, as shown in [fig Fig. 4](#). This is especially true for low ECS models. For instance, the minimum and maximum carbon allocation in the MIROC-ES2L at 2 °C GWL is 1225 PgC in SSP5-8.5 and 1361 PgC in SSP3-7.0. The difference between these two projections of the same model with the same warming level is 136 PgC. For the decade 2008–2017, the mean annual emissions were  $9.4 \pm 0.5$  PgC yr<sup>-1</sup>, so this difference alone is equivalent to [around 13 years of our entire approximately 14 years of the](#) current total global emissions.

[In fig In Fig. 4](#), when comparing individual models between different GWLs, the highest total carbon allocation at the 2 °C GWL is 1521 PgC (NorESM2-LM SSP3-7.0). This is more total carbon than several models emitted at higher GWLs: the lowest carbon emitted at 4 °C GWL was as low as 1220 PgC (for CanESM5-CanOE, in the SSP3-7.0 scenario). In addition, both CanESM5 models and the [UKESM1-UKESM1-0-LL](#) model reached 4 °C of warming in three different scenarios with less atmospheric carbon than NorESM2-LM had when it reached the 2 °C of warming GWL. This highlights the significant role that a model's ECS plays in the uncertainty of warming projections. A model's sensitivity to CO<sub>2</sub> concentration significantly impacts its projection of the total carbon allocation at global warming levels, as well as the absolute values of the individual carbon sinks in the ocean and land.

~~This sensitivity also impacts allowable carbon budgets, and widens the range in the allowable emissions (Lowe and Bernie, 2018). A carbon budget is the remaining carbon that can be emitted before hitting a warming threshold such as the 2 °C GWL. However, we have demonstrated that the time over which that carbon is emitted impacts its warming effect. If the same total carbon were emitted over a longer period, then the resulting warming would be lower. In effect, there is not a direct one-to-one correspondence between emissions and global warming levels in these simulations.~~

The ocean maintains similar allocation percentages across the GWLs, but in [fig Fig. 3](#) there is a small decline in ocean carbon allocation percentage at the highest CO<sub>2</sub> concentration scenarios towards the end of the 21<sup>st</sup> century. This is likely because much of the ocean is forecast to become increasingly stratified in the coming century, which would reduce downwards mixing of CO<sub>2</sub> ([Li et al., 2020; Muilwijk et al., 2023](#)). This reduction in downward mixing combined by the decline in solubility with rising sea surface temperature, causes the overall absorption rate of CO<sub>2</sub> into the ocean to be reduced. The increase in

stratification is caused by warmer surface layers, combined with gradual decline in overturning rates and overall circulation (Thibodeau et al., 2018; Li et al., 2020; Caesar et al., 2021; Sallée et al., 2021). Ocean acidification may also be playing a role  
465 ~~reducing the~~ in reducing the rate of the chemical transition of dissolved CO<sub>2</sub> and thus also slowing uptake (Zeebe, 2012). In combination, these effects act to reduce the rate that absorbed CO<sub>2</sub> is removed from the surface layer. In the ocean, enhanced ocean acidification has a range of effects but has been shown to decrease survival, calcification, growth, development and abundance over a broad range of marine organisms (Kroeker et al., 2013).

While the ocean fraction is more or less consistent throughout the SSP2-4.5, SSP3-7.0 and SSP5-8.5 scenarios at the GWLs,  
470 the land fraction declines over the coming century in ~~fig~~Fig. 3, from 35% at the end of the historical period to 25.3% in SSP2-4.5, 22% in SSP3-7.0 and 17% in SSP5-8.5 at the year 2100. The land fraction is forecast to decline over the coming century in the higher CO<sub>2</sub> concentration scenarios, although the total land carbon allocation increases. There are several possible explanations for this slowdown of uptake. Land ecosystems have been shown to become progressively less efficient at absorbing carbon as levels of atmospheric CO<sub>2</sub> concentrations increase (Wang et al., 2020). The soil respiration could increase due to  
475 warming more than the carbon uptake ~~increase~~ increases due to photosynthetic uptake (Nyberg and Hovenden, 2020). Alternatively the nitrogen limitation could progressively limit photosynthetic uptake (Ågren et al., 2012). The changing climate may impact vegetation growth and photosynthetic uptake via droughts and warming, which moves plants outside the most efficient temperatures for photosynthesis. It is not clear ~~from this work~~ which factors have the largest impact.

The differences in carbon allocations seen here have consequences in the real world. Higher Global warming and higher CO<sub>2</sub>  
480 ~~suppresses global precipitation, as higher temperatures increase both global and regional precipitation changes (Tebaldi et al., 2021)~~ As levels of increases the regional and temporal variability of precipitation (Tebaldi et al., 2021). There is also the direct effect of increasing atmospheric CO<sub>2</sub> concentrations atmosphere increase, land ecosystems globally become progressively less efficient at absorbing carbon (Wang et al., 2020). Higher CO<sub>2</sub> on radiative cooling rates. This impacts the vertical thermal structure of the atmosphere and thus tropical overturning circulations and regional precipitation. This direct effect of atmospheric  
485 CO<sub>2</sub> is independent of the level of warming (Bony et al., 2013). This means that models or scenarios that have a greater atmospheric fraction of CO<sub>2</sub> causes enhanced ocean acidification, which has a range of effects but has been shown to decrease survival, calcification, growth, development and abundance over a broad range of marine organisms (Kroeker et al., 2013).

#### 4.1 ~~Survivor bias and Impact of ECS~~

~~Not all scenarios are expected to reach these warming thresholds before the year 2100. While it is highly likely that all SSP5-8.5~~  
490 ~~will reach 2 C of warming, it is unlikely that any SSP1-1.9 experiments will reach 4 C of warming. This is why the 4 C GWL pane of fig. 2 only includes two multi-model means, while the 2 C GWL pane includes four. On the other hand, in certain combinations of scenario and GWL, it is possible that only some models reach the threshold. For instance, three of the six SSP1-1.9 models reach the 2 C GWL. As described above, the method that we used to populate fig. 2 took the multi-model mean first with all models contributing equally, then used that ensemble mean to calculate the GWL threshold years. An~~  
495 ~~alternative method could first calculate the GWL threshold years for individual ensemble members, then take the mean of only~~

~~those that reach the threshold. This alternative method would implicitly include survivor bias, causing the overall weighting and conclusions to be biased towards high ECS models.~~

500 The SSP1-1.9 scenario includes data from 6 models, yet only three models reach the 2 °C GWL, as can be seen by comparing tab. 1 and fig. 4. Similarly, the SSP2-4.5 scenario includes data from 13 models, yet only two models reach the 4 °C GWL. These missing models would most likely reach the thresholds at some point after the year 2100, if allowed to run for enough additional years with positive net at a given GWL will be more prone to this regional response to changed atmospheric radiative cooling, stability and circulation change, than models or scenarios with a smaller CO<sub>2</sub> emissions fraction in the atmosphere.

#### 4.1 Impact of ECS

505 The ensemble of CMIP6 models has a wide range of ECS values, and ~~their sensitivity to carbon has impacts on this impacts~~ several aspects of carbon allocation. ~~The~~ We show that the GWL threshold year and the total carbon change are both inversely correlated with ECS. ~~Similarly,~~ Similarly, we found that the carbon in the atmosphere and allocated to the ocean are both inversely correlated with ECS. The ECS does not appear to be consistently correlated with the total land carbon allocation or the land carbon fraction at all scenarios and GWLs. The wider uncertainty and challenging nature of land surface carbon modelling is reflected in a broader range of behaviours in land carbon models in CMIP6.

510 The ECS impacts the GWL threshold year, but this range is also affected by ~~the survivor bias described above~~ survivor bias. While we hesitate to draw conclusions from extrapolating the lines of best fit of ~~fig~~ Fig. 5, the line of best fit for the 2 °C GWL threshold year for the SSP1-2.6 scenario crosses the year 2100 at ~~a~~ an ECS equivalent to 3.1 °C. As the likely range of ECS values could be as low as 2.5 °C, this means that a non-trivial part of the ECS-phase space could be excluded by the ScenarioMIP limit of forecasting to the year 2100. ~~Note that with the method we used to calculate the GWL year uses a~~ smoothing window of 21 years, so the last possible GWL threshold year is 2090. While we could extend the analysis with some longer term simulations, very few models and scenarios are available beyond the year 2100. To address this issue, the next round of ScenarioMIP ~~for~~ in CMIP7 could extend its standard cut off beyond the year 2100. This would reduce survivor bias at 2 °C GWL and allow the inclusion of models with a low but still feasible ECS of 2.5 °C.

520 Hausfather et al. (2022) outline a few analysis strategies for addressing the “hot model” problem in CMIP6. The first option is to use the GWL methodology as we have in this work. One of the alternative recommendations is to perform analysis of CMIP6 ensembles without the contributions of models that fall outside the likely ECS range of 2.5 - 4 °C. In our case, this would remove seven of the thirteen models from the analysis, leaving six or fewer models contributing to each scenario. This would be an unnecessarily harsh requirement as we have already demonstrated that using GWL methodology can reduce the impact of the range of ECS relative to the “target year” methodology. In addition, uncertainties in cloud feedbacks have been  
525 identified as the main cause of the large range of ECS (Ceppi and Nowack, 2021), and it is unlikely that there is direct link between a models ability to reproduce cloud feedback behaviour and its ability to reproduce the carbon allocation, as these are independently modelled systems.

We have used the terms effective climate sensitivity and equilibrium climate sensitivity interchangeably. However, they are not the same. Gjermundsen et al. (2021) compared two Earth System models, NorESM2 and CESM2, that had the same

530 atmospheric model but different ocean components. These two models had very different EffCS values but were otherwise very  
similar. NorESM2's EffCS is 2.56 °C and CESM2's EffCS is 5.15 °C. In that work, they found that the greater heat storage at  
depth in NorESM2 delayed the Southern Ocean's surface warming and associated cloud responses, which in turn delayed the  
global mean surface warming. This effect appeared in the 4xCO<sub>2</sub> simulation several centuries after the 150 year cutoff used to  
535 feedback eventually occurs in both models, the same warming is realised, and the two models would show similar equilibrium  
climate sensitivities. The Gregory method for calculating the effective climate sensitivity that was used by Zelinka et al. (2020)  
to generate the ECS values used here does not tell the entire story for the eventually realised warming from a given cumulative  
emission, because it is not fully compatible with the true equilibrium climate sensitivity. It may be possible to take this effect  
into account in future works, for instance, by replacing the surface atmospheric warming anomaly with some measure of the  
540 global volume-weighted mean ocean heat anomaly.

#### 4.2 Anomalous behaviour in SSP3-7.0

The SSP3-7.0 scenario often appears to be an outlier, ~~for~~. For instance, in figs. 2 and 4, it does not conform to the pattern  
of the other scenarios. ~~Also, in fig. 4,~~ In addition, SSP3-7.0 is the scenario showing the widest range of carbon allocation  
behaviours at both the 2 °C and 3 °C GWLs ~~in Fig. 4.~~ The SSP3-7.0 scenario has the highest methane concentration and  
545 air pollution precursor emissions forcing, even higher than those in SSP5-8.5 (Meinshausen et al., 2017, 2020). In the other  
scenarios, the methane and aerosol precursors scale approximately in proportion to the CO<sub>2</sub> concentration. Methane is a strong  
greenhouse gas and has a warming effect, but pollution precursor emissions are linked to aerosols and cloud formation, which  
generally have a cooling effect (Twomey, 1977; Meinshausen et al., 2017). In CMIP6, methane warming can overwhelm,  
be overwhelmed by, or balance with aerosol cooling and the relative strengths of these effects depend strongly on the model  
550 parameterisation choices and ~~there~~ their relative strengths in the scenario forcing. The relative strength of the warming methane  
emissions and the cooling aerosol precursors determines the impact on the warming rate and hence the GWL timing. ~~While in~~  
~~other scenarios the methane and aerosol precursors scale approximately in proportion to the CO<sub>2</sub>,~~ This is why the warming  
in SSP3-7.0 ~~, they are significantly higher. Therefore, SSP3-7.0 scenarios may have a very different warming response to CO<sub>2</sub>~~  
~~than other scenarios, and warming is less closely linked~~ is not as tightly bound to the atmospheric CO<sub>2</sub> concentration ~~. So~~  
555 ~~while as in other scenarios. Even though~~ warming is still correlated to total cumulative emissions, SSP3 scenarios may reach  
the GWLs significantly relatively earlier or later than other scenarios at the same CO<sub>2</sub> concentration. This ~~effort~~ effect could  
be investigated in detail if for instance the SSP3-8.5 or SSP5-7.0 scenarios were simulated.

~~In any case, the~~ The impact of different methane and aerosol precursor emissions on the climate response remains highly  
uncertain in CMIP6. The overall warming impact of methane is not further considered in this work as is it secondary to CO<sub>2</sub>  
560 warming, but it could be examined in future extensions.

### 4.3 Limitations and possible extensions

While the CMIP6 experiments start in 1850 from a pre-industrial control, clearly this is not the starting point for the anthropogenic impact on the land surface or the carbon cycle. ~~Changes to the carbon cycle~~ The human impact on the environment began much earlier and this has implications for ~~ongoing on-going~~ carbon partitioning (Bronse laer et al., 2017; Le Quéré et al., 2018; Friedlingstein et al., 2022). For instance, between 1765 and 1850, atmospheric CO<sub>2</sub> rose by roughly 10 ppm, and accounting for this era resulted in a 4.5% change in ocean uptake in CMIP5 models (Bronse laer et al., 2017).

Similarly, the representation of dynamic vegetation, soil carbon and fire response is most likely under-sampled in this ensemble (Arora et al., 2020; Koch et al., 2021). Notably, CMIP6 models are not capturing present-day tropical forest carbon dynamics; the multi-model mean estimate of the pan-tropical carbon sink is half of the observational estimate (Koch et al., 2021). This uncertainty in the strength of carbon–concentration and carbon–climate feedbacks over land is well ~~known~~ (Cox et al., 2000; Friedlingstein et al., 2006; Arora et al., 2013). ~~established~~ (Cox et al., 2000; Friedlingstein et al., 2006; Arora et al., 2013).

The global ocean carbon inventory is also affected by the land-to-ocean carbon flux from river runoff and the carbon burial in ocean sediments, which is not represented in our ensemble (Arora et al., 2020). The flux of land carbon into the ocean via rivers is between  $0.45 \pm 0.18$  PgC yr<sup>-1</sup> and  $0.78 \pm 0.41$  PgC yr<sup>-1</sup> and is generally not considered in ESMs (Jacobson et al., 2007; Resplandy et al., 2018; Hauck et al., 2020). Including the riverine flux of particulate and dissolved organic carbon would require models to represent both estuarine and shallow shelf processes. This would most likely require higher model resolutions and computational costs.

~~In this~~ One of the limitations of the GWL methodology is that it focuses on the realised warming at a specific point in time. This is the transient warming, and it is unlikely that this warming includes the full effect of all cumulative CO<sub>2</sub> emissions. In effect, the CO<sub>2</sub> emissions have not yet played out to equilibrium at the GWL, and there is likely to be a continued delay in their warming effect.

Not all scenarios are expected to reach these warming thresholds before the year 2100. For instance, while it is highly likely that all SSP5-8.5 simulations will reach 2 °C of warming, it is unlikely that any SSP1-1.9 experiments will reach 4 °C of warming. On the other hand, only some of the models reach the threshold in certain combinations of scenario and GWL. For instance, three of the six SSP1-1.9 models reach the 2 °C GWL. These missing models would most likely reach the thresholds at some point after the year 2100, if allowed to run for enough additional years with positive net CO<sub>2</sub> emissions. Future works could potentially extend their analysis by including the long-timeline scenarios beyond the year 2100. The method that we used to populate Fig. 2 took the multi-model mean first with all models contributing equally, then used that ensemble mean to calculate the GWL threshold years. An alternative method could first calculate the GWL threshold years for individual ensemble members, then take the mean of only those that reach the threshold. However, this alternative method would implicitly include survivor bias, causing the overall weighting and conclusions to be biased towards high ECS models.

In this work, we used concentration driven scenarios instead of emission driven scenarios. Emission driven scenarios allow significantly more flexibility in the behaviour of the atmospheric carbon, ~~in effect~~. In practice, this would be like adding a

595 third degree of freedom into the [total carbon allocation](#) calculation. Although a limited set of emission driven runs exist, it was found that there are actually very few differences in simulated temperature or atmospheric CO<sub>2</sub> concentration between concentration driven and emission driven scenarios (Lee et al., 2021, Sec. 4.3.1.1). In any case, several key datasets required in the calculation of the land use emissions (~~LUE~~) [in eq. 1](#) were not available in the emission driven experiments at the time of writing.

600 In [Fig. 3](#), the multi-model mean of both SSP1 scenarios shows signs of recovery and carbon drawdown, [but no datasets in this analysis drop below the 2 °C GWL threshold](#). In future ~~versions of this work~~ [studies](#), it would be interesting to examine ~~whether the carbon allocation behaves similarly on the way down as it did on the way up.~~ [the reversibility of carbon allocation with negative emission forcing scenarios](#). More generally, extension simulations beyond 2100 would be valuable for studying how patterns of carbon allocation change as emissions decline past ~~net-zero~~ [net-zero](#).

605 ~~While we made every effort to build a uniform ensemble, ScenarioMIP's flexible contributions means that we have a diversity in data occupancy between scenarios. The SSP5-8.5 ensemble has the highest mean ECS, meaning that the multi-model mean of this ensemble will likely be warmer than other scenarios multi-model mean's at the same atmospheric carbon concentration. Similarly, we were fortunate that the mean ECS of our SSP1-1.9 ensemble falls in a similar range to the other scenarios, despite it containing significantly fewer models than the other scenarios. While the impact of ensemble bias is a small effect here, the multi-model means could have had a much wider range of mean ECS values between scenario groups. In the future, any investigation using the multi-model means needs to be careful with handling the equilibrium climate sensitivity bias of the ensemble. Two ensembles constituted of differing sets of models may not always be directly comparable.~~

610 In [fig 5](#), we generated a fit to each ~~datasat~~ [dataset](#) against the ECS. This fit is built on the assumption that these behaviours are linear and that the straight line fit is a reasonable approximation of their behaviour. However, as can be seen in this figure, this is not true in all cases. Several of the datasets have non-linear behaviours with regards to ECS. It may be possible to expand upon this work and generate more complex fits to these datasets to estimate the behaviour of these models within the likely ECS range of 2.5 ~~-4-~~ [4](#) °C.

620 [In this work, we attempt to maximise the number of models. ScenarioMIP's flexible contributions means that each scenario's ensemble is composed of a different set of models, as shown in Table 1. This diversity results in a different mean ECS for each scenario. We were fortunate that the range of the mean ECS values was only 0.21 °C, despite for instance SSP1-1.9 containing significantly fewer models than the other scenarios. A different set of models could conceivably result in a wider range of mean ECS values between scenarios, which would impact the warming rates at the same CO<sub>2</sub> concentrations, making interpretation more challenging and potentially introducing bias in the conclusions. In future investigations of CMIP multi-model means using the GWL methodology, the mean equilibrium climate sensitivity of each ensemble should be included alongside the analysis as two ensembles constituted of differing sets of models may not always be directly comparable.](#)

625



## 5 Conclusions

Using an ensemble of CMIP6 simulations, we have ~~shown that~~ quantified how the carbon allocation between Earth ~~system~~ System components differs between scenarios after the same change in global mean surface temperature anomaly. Scenarios with higher carbon concentrations reach the global warming levels sooner, and have proportionally less carbon allocated to the ocean and land surface at that time than scenarios with lower emissions. The differences in estimated carbon emissions between scenarios vary even at the same GWL, and can be equivalent to several years' worth of global total emissions. ~~These result appear as~~ This is a result of the GWL methodology, but our conclusions are nevertheless compatible with previous works and we do not claim to refute previous target year analyses.

A model's sensitivity to CO<sub>2</sub> concentration significantly affects its total carbon allocation between the atmosphere, ocean and land at all global warming levels. However, our CMIP6 ensemble contains many models that fall outside the likely ECS range of 2.5 - ~~4~~ 4 °C. By using the GWL methodology, we can exploit the full CMIP6 ensemble and weight each model equally, without excluding the so-called "hot models". We did not find a consistent relationship between ECS and any of the fractional carbon allocations. However, we did demonstrate that ECS and total carbon allocation are ~~correlated~~ related. Models with lower sensitivity to carbon reach the GWL with more carbon in the individual reservoirs and more carbon overall. This is because it takes low ECS models longer to reach the same warming level, allowing more time for carbon to accumulate in the Earth ~~system~~ System.

In addition to the impacts of ECS and total atmospheric carbon concentration, the distinct characteristics of each scenario pathway also influences the carbon allocation. The SSP3-7.0 scenario includes ~~methane-induced~~ both high methane-induced warming and high pollution precursors cooling ~~impacts~~, and the strength of these effects are model specific and not directly related to ECS. These environmental forcings in SSP3-7.0 can generate a very different warming response, GWL threshold year and carbon allocation than scenarios where CO<sub>2</sub>, methane and pollution precursors all scale with historical values.

Ultimately, across all model simulations, a significant rise in global mean surface temperature is projected over the 21<sup>st</sup> century. This underscores the need for an accelerating transition to low carbon technologies to reduce the risk of the worst effects of climate change.

*Code and data availability.* This analysis was performed using ESMValTool and the exact software tools used in this manuscript are available via zenodo: 10.5281/zenodo.8335060, version 1.1. The main ESMValTool recipe is `recipe_gwt_time_series_CMIP6_2022_all.yml` in the `esmvaltool/recipes` directory, and the main diagnostic script is `diagnostic_gwt_timeseries.py` in the `esmvaltool/diag_scripts/ocean` directory. An up-to-date version of the base ESMValTool system is available on github: [github.com/ESMValGroup](https://github.com/ESMValGroup) which includes up to date code, documentation and tutorials. CMIP6 climate model data used in this paper was obtained from the CEDA's Earth System Federation Grid node, but is widely available elsewhere: <https://esgf-node.llnl.gov/search/cmip6/>

*Video supplement.* A video abstract for this paper is available here: [path-to-be-confirmed](#).

*Author contributions.* All authors contributed to the writing, discussion, initial outline, literature survey and editorial feedback of the manuscript. LdM led the work, performed the analyses and led the writing. RS, CGJ, LdM developed the GWL analysis methods. CDJ, SL, TQ contributed to the land surface carbon calculation. JW contributed to the extraction and curation of the model data. CGJ, JB, led the  
660 UKESM1 and TerraFirma projects and working groups where this work was funded.

*Competing interests.* The authors are not aware of any competing interests.

*Acknowledgements.* LdM and DIK were supported by the UK Natural Environment Research Council through The UK Earth System Modelling Project (UKESM, grant no. NE/N017951/1). RS, RJP, TQ and RPA are funded by the UK National Centre for Earth Observation (NE/N018079/1). LdM, RS, JB, RJP, CDJ, CGJ, AY were supported by the UK Natural Environment Research Council through the TerraFIRMA: Future Impacts, Risks and Mitigation Actions in a changing Earth ~~system~~System project, Grant reference NE/W004895/1. CGJ acknowledges funding from the NERC National Capability UKESM grant no. NE/N017978/1 and EU Horizon 2020 project CRESCENDO, grant number: 641816. CDJ, SL and JW were supported by the Joint UK BEIS/Defra Met Office Hadley Centre Climate Programme (GA01101). CDJ was supported by the European Union's Horizon 2020 research and innovation programme under Grant Agreement No 101003536 (ESM2025 - Earth System Models for the Future). The authors would like to acknowledge use of the Centre for Environmental  
670 Data Analysis (CEDA) JASMIN computing cluster and BADC data centres in this work. The authors would also like to thank the JASMIN and ESMValTool teams for their assistance with this work. The authors would also like to acknowledge anonymous reviewer #1 and Dr. John Dunne for their patience and contributions towards the final manuscript.

## References

- 675 Ågren, G. I., Wetterstedt, J. A. M., and Billberger, M. F. K.: Nutrient limitation on terrestrial plant growth – modeling the interaction between nitrogen and phosphorus, *New Phytologist*, 194, 953–960, <https://doi.org/10.1111/j.1469-8137.2012.04116.x>, 2012.
- Allen, M. R., Frame, D. J., Huntingford, C., Jones, C. D., Lowe, J. A., Meinshausen, M., and Meinshausen, N.: Warming caused by cumulative carbon emissions towards the trillionth tonne, *Nature*, 458, 1163–1166, <https://doi.org/10.1038/nature08019>, 2009.
- Arias, P., Bellouin, N., Coppola, E., Jones, R., Krinner, G., Marotzke, J., Naik, V., Palmer, M., Plattner, G.-K., Rogelj, J., Rojas, M., Sillmann, J., Storelvmo, T., Thorne, P., Trewin, B., Achuta Rao, K., Adhikary, B., Allan, R., Armour, K., Bala, G., Barimalala, R., Berger, S.,  
680 Canadell, J., Cassou, C., Cherchi, A., Collins, W., Collins, W., Connors, S., Corti, S., Cruz, F., Dentener, F., Dereczynski, C., Di Luca, A., Diongue Niang, A., Doblas-Reyes, F., Dosio, A., Douville, H., Engelbrecht, F., Eyring, V., Fischer, E., Forster, P., Fox-Kemper, B., Fuglestedt, J., Fyfe, J., Gillett, N., Goldfarb, L., Gorodetskaya, I., Gutierrez, J., Hamdi, R., Hawkins, E., Hewitt, H., Hope, P., Islam, A., Jones, C., Kaufman, D., Kopp, R., Kosaka, Y., Kossin, J., Krakovska, S., Lee, J.-Y., Li, J., Mauritsen, T., Maycock, T., Meinshausen, M., Min, S.-K., Monteiro, P., Ngo-Duc, T., Otto, F., Pinto, I., Pirani, A., Raghavan, K., Ranasinghe, R., Ruane, A., Ruiz, L., Sallée, J.-B.,  
685 Samset, B., Sathyendranath, S., Seneviratne, S., Sörensson, A., Szopa, S., Takayabu, I., Tréguier, A.-M., van den Hurk, B., Vautard, R., von Schuckmann, K., Zaehle, S., Zhang, X., and Zickfeld, K.: *Climate Change 2021: The Physical Science Basis. Contribution of Working Group I to the Sixth Assessment Report of the Intergovernmental Panel on Climate Change: Technical Summary*, p. 33-144, Cambridge University Press, Cambridge, United Kingdom and New York, NY, USA, <https://doi.org/10.1017/9781009157896.002>, 2021.
- Arora, V. K., Boer, G. J., Friedlingstein, P., Eby, M., Jones, C. D., Christian, J. R., Bonan, G., Bopp, L., Brovkin, V., Cadule, P., Hajima, T.,  
690 Ilyina, T., Lindsay, K., Tjiputra, J. F., and Wu, T.: Carbon–Concentration and Carbon–Climate Feedbacks in CMIP5 Earth System Models, *Journal of Climate*, 26, 5289 – 5314, <https://doi.org/10.1175/JCLI-D-12-00494.1>, 2013.
- Arora, V. K., Katavouta, A., Williams, R. G., Jones, C. D., Brovkin, V., Friedlingstein, P., Schwinger, J., Bopp, L., Boucher, O., Cadule, P., Chamberlain, M. A., Christian, J. R., Delire, C., Fisher, R. A., Hajima, T., Ilyina, T., Joetzjer, E., Kawamiya, M., Koven, C. D., Krasting, J. P., Law, R. M., Lawrence, D. M., Lenton, A., Lindsay, K., Pongratz, J., Raddatz, T., Séférian, R., Tachiiri, K., Tjiputra, J. F., Wiltshire, A., Wu, T., and Ziehn, T.: Carbon–concentration and carbon–climate feedbacks in CMIP6 models and their comparison to CMIP5 models, *Biogeosciences*, 17, 4173–4222, <https://doi.org/10.5194/bg-17-4173-2020>, 2020.
- Bony, S., Bellon, G., Klocke, D., Sherwood, S., Fermepin, S., and Denvil, S.: Robust direct effect of carbon dioxide on tropical circulation and regional precipitation, *Nature Geoscience*, 6, 447–451, <https://doi.org/10.1038/ngeo1799>, 2013.
- Boucher, O., Servonnat, J., Albright, A. L., Aumont, O., Balkanski, Y., Bastrikov, V., Bekki, S., Bonnet, R., Bony, S., Bopp, L., Braconnot, P., Brockmann, P., Cadule, P., Caubel, A., Cheruy, F., Codron, F., Cozic, A., Cugnet, D., D’Andrea, F., Davini, P., de Lavergne, C., Denvil, S., Deshayes, J., Devilliers, M., Ducharne, A., Dufresne, J.-L., Dupont, E., Éthé, C., Fairhead, L., Falletti, L., Flavoni, S., Foujols, M.-A., Gardoll, S., Gastineau, G., Ghattas, J., Grandpeix, J.-Y., Guenet, B., Guez, Lionel, E., Guilyardi, E., Guimberteau, M., Hauglustaine, D., Hourdin, F., Idelkadi, A., Joussaume, S., Kageyama, M., Khodri, M., Krinner, G., Lebas, N., Levavasseur, G., Lévy, C., Li, L., Lott, F., Lurton, T., Luyssaert, S., Madec, G., Madeleine, J.-B., Maignan, F., Marchand, M., Marti, O., Mellul, L., Meurdesoif, Y., Mignot, J., Musat,  
700 I., Otlé, C., Peylin, P., Planton, Y., Polcher, J., Rio, C., Rochetin, N., Rousset, C., Sepulchre, P., Sima, A., Swingedouw, D., Thiéblemont, R., Traore, A. K., Vancoppenolle, M., Vial, J., Vialard, J., Viovy, N., and Vuichard, N.: Presentation and Evaluation of the IPSL-CM6A-LR Climate Model, *Journal of Advances in Modeling Earth Systems*, 12, e2019MS002 010, <https://doi.org/10.1029/2019MS002010>, 2020.
- Bronselaer, B., Winton, M., Russell, J., Sabine, C. L., and Khatiwala, S.: Agreement of CMIP5 Simulated and Observed Ocean Anthropogenic CO<sub>2</sub> Uptake, *Geophysical Research Letters*, 44, 12,298–12,305, <https://doi.org/10.1002/2017GL074435>, 2017.

- 710 Brunner, L., Pendergrass, A. G., Lehner, F., Merrifield, A. L., Lorenz, R., and Knutti, R.: Reduced global warming from CMIP6 projections when weighting models by performance and independence, *Earth System Dynamics*, 11, 995–1012, <https://doi.org/10.5194/esd-11-995-2020>, 2020.
- Burton, C., Kelley, D. I., Jones, C. D., Betts, R. A., Cardoso, M., and Anderson, L.: South American fires and their impacts on ecosystems increase with continued emissions, *Climate Resilience and Sustainability*, 1, e8, <https://doi.org/10.1002/cli2.8>, 2022.
- 715 Caesar, L., McCarthy, G. D., Thornalley, D. J. R., Cahill, N., and Rahmstorf, S.: Current Atlantic Meridional Overturning Circulation weakest in last millennium, *Nature Geoscience*, 14, 118–120, <https://doi.org/10.1038/s41561-021-00699-z>, 2021.
- Caldeira, K. and Wickett, M. E.: Anthropogenic carbon and ocean pH, *Nature*, 425, 365–365, <https://doi.org/10.1038/425365a>, 2003.
- Canadell, J., Monteiro, P., Costa, M., Cotrim da Cunha, L., Cox, P., Eliseev, A., Henson, S., Ishii, M., Jaccard, S., Koven, C., Lohila, A., Patra, P., Piao, S., Rogelj, J., Syampungani, S., Zaehle, S., and Zickfeld, K.: *Global Carbon and other Biogeochemical Cycles and Feedbacks*, p. 673–816, Cambridge University Press, Cambridge, United Kingdom and New York, NY, USA, <https://doi.org/10.1017/9781009157896.007>, 2021.
- 720 Ceppi, P. and Nowack, P.: Observational evidence that cloud feedback amplifies global warming, *Proceedings of the National Academy of Sciences*, 118, e2026290 118, <https://doi.org/10.1073/pnas.2026290118>, 2021.
- Christian, J. R., Denman, K. L., Hayashida, H., Holdsworth, A. M., Lee, W. G., Riche, O. G. J., Shao, A. E., Steiner, N., and Swart, N. C.: Ocean biogeochemistry in the Canadian Earth System Model version 5.0.3: CanESM5 and CanESM5-CanOE, *Geoscientific Model Development*, 15, 4393–4424, <https://doi.org/10.5194/gmd-15-4393-2022>, 2022.
- 725 Cox, P. M., Betts, R. A., Jones, C. D., Spall, S. A., and Totterdell, I. J.: Acceleration of global warming due to carbon-cycle feedbacks in a coupled climate model, *Nature*, 408, 184–187, <https://doi.org/10.1038/35041539>, 2000.
- Danabasoglu, G., Lamarque, J.-F., Bacmeister, J., Bailey, D. A., DuVivier, A. K., Edwards, J., Emmons, L. K., Fasullo, J., Garcia, R., Gettelman, A., Hannay, C., Holland, M. M., Large, W. G., Lauritzen, P. H., Lawrence, D. M., Lenaerts, J. T. M., Lindsay, K., Lipscomb, W. H., Mills, M. J., Neale, R., Oleson, K. W., Otto-Bliesner, B., Phillips, A. S., Sacks, W., Tilmes, S., van Kampenhout, L., Vertenstein, M., Bertini, A., Dennis, J., Deser, C., Fischer, C., Fox-Kemper, B., Kay, J. E., Kinnison, D., Kushner, P. J., Larson, V. E., Long, M. C., Mickelson, S., Moore, J. K., Nienhouse, E., Polvani, L., Rasch, P. J., and Strand, W. G.: The Community Earth System Model Version 2 (CESM2), *Journal of Advances in Modeling Earth Systems*, 12, e2019MS001 916, <https://doi.org/10.1029/2019MS001916>, 2020.
- 730 Dunne, J. P., Horowitz, L. W., Adcroft, A. J., Ginoux, P., Held, I. M., John, J. G., Krasting, J. P., Malyshev, S., Naik, V., Paulot, F., Shevliakova, E., Stock, C. A., Zadeh, N., Balaji, V., Blanton, C., Dunne, K. A., Dupuis, C., Durachta, J., Dussin, R., Gauthier, P. P. G., Griffies, S. M., Guo, H., Hallberg, R. W., Harrison, M., He, J., Hurlin, W., McHugh, C., Menzel, R., Milly, P. C. D., Nikonov, S., Paynter, D. J., Ploshay, J., Radhakrishnan, A., Rand, K., Reichl, B. G., Robinson, T., Schwarzkopf, D. M., Sentman, L. T., Underwood, S., Vahlenkamp, H., Winton, M., Wittenberg, A. T., Wyman, B., Zeng, Y., and Zhao, M.: The GFDL Earth System Model Version 4.1 (GFDL-ESM 4.1): Overall
- 740 Coupled Model Description and Simulation Characteristics, *Journal of Advances in Modeling Earth Systems*, 12, e2019MS002 015, <https://doi.org/10.1029/2019MS002015>, 2020.
- Erda, L., Wei, X., Hui, J., Yinlong, X., Yue, L., Liping, B., and Liyong, X.: Climate change impacts on crop yield and quality with CO<sub>2</sub> fertilization in China., *Philos Trans R Soc Lond B Biol Sci.*, 360, 2149 – 2154, <https://doi.org/doi/10.1098/rstb.2005.1743>, 2005.
- Eyring, V., Bony, S., Meehl, G. A., Senior, C. A., Stevens, B., Stouffer, R. J., and Taylor, K. E.: Overview of the Coupled Model Intercomparison Project Phase 6 (CMIP6) experimental design and organization, *Geoscientific Model Development*, 9, 1937–1958, <https://doi.org/10.5194/gmd-9-1937-2016>, 2016.

- Flynn, C. M. and Mauritsen, T.: On the climate sensitivity and historical warming evolution in recent coupled model ensembles, *Atmospheric Chemistry and Physics*, 20, 7829–7842, <https://doi.org/10.5194/acp-20-7829-2020>, 2020.
- 750 Friedlingstein, P., Cox, P., Betts, R., Bopp, L., von Bloh, W., Brovkin, V., Cadule, P., Doney, S., Eby, M., Fung, I., Bala, G., John, J., Jones, C., Joos, F., Kato, T., Kawamiya, M., Knorr, W., Lindsay, K., Matthews, H. D., Raddatz, T., Rayner, P., Reick, C., Roeckner, E., Schnitzler, K.-G., Schnur, R., Strassmann, K., Weaver, A. J., Yoshikawa, C., and Zeng, N.: Climate–Carbon Cycle Feedback Analysis: Results from the C4MIP Model Intercomparison, *Journal of Climate*, 19, 3337 – 3353, <https://doi.org/10.1175/JCLI3800.1>, 2006.
- 755 Friedlingstein, P., O’Sullivan, M., Jones, M., Andrew, R., Gregor, L., Hauck, J., Le Quéré, C., Luijkx, I., Olsen, A., Peters, G., Peters, W., Pongratz, J., Schwingshackl, C., Sitch, S., Canadell, J., Ciais, P., Jackson, R., Alin, S., Alkama, R., and Zheng, B.: Global Carbon Budget 2022, *Earth System Science Data*, 14, 4811–4900, <https://doi.org/10.5194/essd-14-4811-2022>, 2022.
- Friend, A. D., Lucht, W., Rademacher, T. T., Keribin, R., Betts, R., Cadule, P., Ciais, P., Clark, D. B., Dankers, R., Falloon, P. D., Ito, A., Kahana, R., Kleidon, A., Lomas, M. R., Nishina, K., Ostberg, S., Pavlick, R., Peylin, P., Schaphoff, S., Vuichard, N., Warszawski, L., Wiltshire, A., and Woodward, F. I.: Carbon residence time dominates uncertainty in terrestrial vegetation responses to future climate and atmospheric CO<sub>2</sub>, *Proceedings of the National Academy of Sciences*, 111, 3280–3285, <https://doi.org/10.1073/pnas.1222477110>, 2014.
- 760 Gjermundsen, A., Nummelin, A., Olivie, D., Bentsen, M., Seland, Ø., and Schulz, M.: Shutdown of Southern Ocean convection controls long-term greenhouse gas-induced warming, *Nature Geoscience*, 14, 724–731, <https://doi.org/10.1038/s41561-021-00825-x>, 2021.
- Gregory, J. M., Ingram, W. J., Palmer, M. A., Jones, G. S., Stott, P. A., Thorpe, R. B., Lowe, J. A., Johns, T. C., and Williams, K. D.: A new method for diagnosing radiative forcing and climate sensitivity, *Geophysical Research Letters*, 31, <https://doi.org/10.1029/2003GL018747>, 2004.
- 765 Hajima, T., Watanabe, M., Yamamoto, A., Tatebe, H., Noguchi, M. A., Abe, M., Ohgaito, R., Ito, A., Yamazaki, D., Okajima, H., Ito, A., Takata, K., Ogochi, K., Watanabe, S., and Kawamiya, M.: Development of the MIROC-ES2L Earth system model and the evaluation of biogeochemical processes and feedbacks, *Geoscientific Model Development*, 13, 2197–2244, <https://doi.org/10.5194/gmd-13-2197-2020>, 2020.
- Hansen, J., Johnson, D., Lacis, A., Lebedeff, S., Lee, P., Rind, D., and Russell, G.: Climate Impact of Increasing Atmospheric Carbon Dioxide, *Science*, 213, 957–966, <https://doi.org/10.1126/science.213.4511.957>, 1981.
- 770 Hauck, J., Zeising, M., Le Quéré, C., Gruber, N., Bakker, D. C. E., Bopp, L., Chau, T. T. T., Gurses, O., Ilyina, T., Landschützer, P., Lenton, A., Resplandy, L., Rödenbeck, C., Schwinger, J., and Séférian, R.: Consistency and Challenges in the Ocean Carbon Sink Estimate for the Global Carbon Budget, *Frontiers in Marine Science*, 7, <https://doi.org/10.3389/fmars.2020.571720>, 2020.
- Hausfather, Z., Marvel, K., Schmidt, G. A., Nielsen-Gammon, J. W., and Zelinka, M.: Climate simulations: Recognize the ‘hot model’ problem, *Nature*, 605, 26–29, <https://doi.org/10.1038/d41586-022-01192-2>, 2022.
- 775 Heuzé, C.: Antarctic Bottom Water and North Atlantic Deep Water in CMIP6 models, *Ocean Science*, 17, 59–90, <https://doi.org/10.5194/os-17-59-2021>, 2021.
- Hilmi, N., Chami, R., Sutherland, M. D., Hall-Spencer, J. M., Lebleu, L., Benitez, M. B., and Levin, L. A.: The Role of Blue Carbon in Climate Change Mitigation and Carbon Stock Conservation, *Frontiers in Climate*, 3, <https://doi.org/10.3389/fclim.2021.710546>, 2021.
- 780 IPCC: Climate Change 2021: The Physical Science Basis. Contribution of Working Group I to the Sixth Assessment Report of the Intergovernmental Panel on Climate Change, vol. In Press, Cambridge University Press, Cambridge, United Kingdom and New York, NY, USA, <https://doi.org/10.1017/9781009157896>, 2021a.
- IPCC: Summary for Policymakers, p. 3-32, Cambridge University Press, Cambridge, United Kingdom and New York, NY, USA, <https://doi.org/10.1017/9781009157896.001>, 2021b.

- 785 Jacobson, A. R., Mikaloff Fletcher, S. E., Gruber, N., Sarmiento, J. L., and Gloor, M.: A joint atmosphere-ocean inversion for surface fluxes of carbon dioxide: 2. Regional results, *Global Biogeochemical Cycles*, 21, <https://doi.org/10.1029/2006GB002703>, 2007.
- Jiang, L., Yan, Y., Hararuk, O., Mickle, N., Xia, J., Shi, Z., Tjiputra, J., Wu, T., and Luo, Y.: Scale-Dependent Performance of CMIP5 Earth System Models in Simulating Terrestrial Vegetation Carbon, *Journal of Climate*, 28, 5217 – 5232, <https://doi.org/10.1175/JCLI-D-14-00270.1>, 2015.
- 790 Jiang, L., Liang, J., Lu, X., Hou, E., Hoffman, F. M., and Luo, Y.: Country-level land carbon sink and its causing components by the middle of the twenty-first century, *Ecological Processes*, 10, 61, <https://doi.org/10.1186/s13717-021-00328-y>, 2021.
- Jiang, L.-Q., Carter, B. R., Feely, R. A., Lauvset, S. K., and Olsen, A.: Surface ocean pH and buffer capacity: past, present and future, *Scientific Reports*, 9, 18 624, <https://doi.org/10.1038/s41598-019-55039-4>, 2019.
- Jones, C., Robertson, E., Arora, V., Friedlingstein, P., Shevliakova, E., Bopp, L., Brovkin, V., Hajima, T., Kato, E., Kawamiya, M., Liddicoat, S., Lindsay, K., Reick, C. H., Roelandt, C., Segschneider, J., and Tjiputra, J.: Twenty-First-Century Compatible CO<sub>2</sub> Emissions and Airborne Fraction Simulated by CMIP5 Earth System Models under Four Representative Concentration Pathways, *Journal of Climate*, 26, 4398 – 4413, <https://doi.org/10.1175/JCLI-D-12-00554.1>, 2013.
- 795 Jones, C. D., Hughes, J. K., Bellouin, N., Hardiman, S. C., Jones, G. S., Knight, J., Liddicoat, S., O'Connor, F. M., Andres, R. J., Bell, C., Boo, K.-O., Bozzo, A., Butchart, N., Cadule, P., Corbin, K. D., Doutriaux-Boucher, M., Friedlingstein, P., Gornall, J., Gray, L., Halloran, P. R., Hurtt, G., Ingram, W. J., Lamarque, J.-F., Law, R. M., Meinshausen, M., Osprey, S., Palin, E. J., Parsons Chini, L., Raddatz, T., Sanderson, M. G., Sellar, A. A., Schurer, A., Valdes, P., Wood, N., Woodward, S., Yoshioka, M., and Zerroukat, M.: The HadGEM2-ES implementation of CMIP5 centennial simulations, *Geoscientific Model Development*, 4, 543–570, <https://doi.org/10.5194/gmd-4-543-2011>, 2011.
- 800 Jones, C. D., Arora, V., Friedlingstein, P., Bopp, L., Brovkin, V., Dunne, J., Graven, H., Hoffman, F., Ilyina, T., John, J. G., Jung, M., Kawamiya, M., Koven, C., Pongratz, J., Raddatz, T., Randerson, J. T., and Zaehle, S.: C4MIP – The Coupled Climate–Carbon Cycle Model Intercomparison Project: experimental protocol for CMIP6, *Geoscientific Model Development*, 9, 2853–2880, <https://doi.org/10.5194/gmd-9-2853-2016>, 2016.
- Katavouta, A. and Williams, R. G.: Ocean carbon cycle feedbacks in CMIP6 models: contributions from different basins, *Biogeosciences*, 18, 3189–3218, <https://doi.org/10.5194/bg-18-3189-2021>, 2021.
- 810 Koch, A., Hubau, W., and Lewis, S. L.: Earth System Models Are Not Capturing Present-Day Tropical Forest Carbon Dynamics, *Earth's Future*, 9, e2020EF001 874, <https://doi.org/10.1029/2020EF001874>, 2021.
- Kroeker, K. J., Kordas, R. L., Crim, R., Hendriks, I. E., Ramajo, L., Singh, G. S., Duarte, C. M., and Gattuso, J.-P.: Impacts of ocean acidification on marine organisms: quantifying sensitivities and interaction with warming, *Global Change Biology*, 19, 1884–1896, <https://doi.org/10.1111/gcb.12179>, 2013.
- 815 Lawrence, D. M., Hurtt, G. C., Arneth, A., Brovkin, V., Calvin, K. V., Jones, A. D., Jones, C. D., Lawrence, P. J., de Noblet-Ducoudré, N., Pongratz, J., Seneviratne, S. I., and Shevliakova, E.: The Land Use Model Intercomparison Project (LUMIP) contribution to CMIP6: rationale and experimental design, *Geoscientific Model Development*, 9, 2973–2998, <https://doi.org/10.5194/gmd-9-2973-2016>, 2016.
- Lawrence, M. G., Schäfer, S., Muri, H., Scott, V., Oschlies, A., Vaughan, N. E., Boucher, O., Schmidt, H., Haywood, J., and Scheffran, J.: Evaluating climate geoengineering proposals in the context of the Paris Agreement temperature goals, *Nature Communications*, 9, 3734, <https://doi.org/10.1038/s41467-018-05938-3>, 2018.
- 820 Le Quéré, C., Andrew, R. M., Friedlingstein, P., Sitch, S., Hauck, J., Pongratz, J., Pickers, P. A., Korsbakken, J. I., Peters, G. P., Canadell, J. G., Arneth, A., Arora, V. K., Barbero, L., Bastos, A., Bopp, L., Chevallier, F., Chini, L. P., Ciais, P., Doney, S. C., Gkritzalis, T., Goll,

- D. S., Harris, I., Haverd, V., Hoffman, F. M., Hoppema, M., Houghton, R. A., Hurtt, G., Ilyina, T., Jain, A. K., Johannessen, T., Jones, C. D., Kato, E., Keeling, R. F., Goldewijk, K. K., Landschützer, P., Lefèvre, N., Lienert, S., Liu, Z., Lombardozi, D., Metzl, N., Munro, D. R., Nabel, J. E. M. S., Nakaoka, S., Neill, C., Olsen, A., Ono, T., Patra, P., Peregon, A., Peters, W., Peylin, P., Pfeil, B., Pierrot, D., Poulter, B., Rehder, G., Resplandy, L., Robertson, E., Rocher, M., Rödenbeck, C., Schuster, U., Schwinger, J., Séférian, R., Skjelvan, I., Steinhoff, T., Sutton, A., Tans, P. P., Tian, H., Tilbrook, B., Tubiello, F. N., van der Laan-Luijkx, I. T., van der Werf, G. R., Viovy, N., Walker, A. P., Wiltshire, A. J., Wright, R., Zaehle, S., and Zheng, B.: Global Carbon Budget 2018, *Earth System Science Data*, 10, 2141–2194, <https://doi.org/10.5194/essd-10-2141-2018>, 2018.
- 825 Lee, J.-Y., Marotzke, J., Bala, G., Cao, L., Corti, S., Dunne, J., Engelbrecht, F., Fischer, E., Fyfe, J., Jones, C., Maycock, A., Mutemi, J., Ndiaye, O., Panickal, S., and Zhou, T.: Future Global Climate: Scenario-Based Projections and Near-Term Information, p. 553–672, Cambridge University Press, Cambridge, United Kingdom and New York, NY, USA, <https://doi.org/10.1017/9781009157896.006>, 2021.
- Li, G., Cheng, L., Zhu, J., Trenberth, K. E., Mann, M. E., and Abraham, J. P.: Increasing ocean stratification over the past half-century, *Nature Climate Change*, 10, 1116–1123, <https://doi.org/10.1038/s41558-020-00918-2>, 2020.
- 835 Liddicoat, S. K., Wiltshire, A. J., Jones, C. D., Arora, V. K., Brovkin, V., Cadule, P., Hajima, T., Lawrence, D. M., Pongratz, J., Schwinger, J., Séférian, R., Tjiputra, J. F., and Ziehn, T.: Compatible Fossil Fuel CO<sub>2</sub> Emissions in the CMIP6 Earth System Models’ Historical and Shared Socioeconomic Pathway Experiments of the Twenty-First Century, *Journal of Climate*, 34, 2853 – 2875, <https://doi.org/10.1175/JCLI-D-19-0991.1>, 2021.
- Lovato, T., Peano, D., Butenschön, M., Materia, S., Iovino, D., Scoccimarro, E., Fogli, P. G., Cherchi, A., Bellucci, A., Gualdi, S., Masina, S., and Navarra, A.: CMIP6 Simulations With the CMCC Earth System Model (CMCC-ESM2), *Journal of Advances in Modeling Earth Systems*, 14, e2021MS002814, <https://doi.org/10.1029/2021MS002814>, 2022.
- 840 Lowe, J. A. and Bernie, D.: The impact of Earth system feedbacks on carbon budgets and climate response, *Philosophical Transactions of the Royal Society A: Mathematical, Physical and Engineering Sciences*, 376, 20170263, <https://doi.org/10.1098/rsta.2017.0263>, 2018.
- Macreadie, P. I., Anton, A., Raven, J. A., Beaumont, N., Connolly, R. M., Friess, D. A., Kelleway, J. J., Kennedy, H., Kuwae, T., Lavery, P. S., Lovelock, C. E., Smale, D. A., Apostolaki, E. T., Atwood, T. B., Baldock, J., Bianchi, T. S., Chmura, G. L., Eyre, B. D., Fourqurean, J. W., Hall-Spencer, J. M., Huxham, M., Hendriks, I. E., Krause-Jensen, D., Laffoley, D., Luisetti, T., Marbà, N., Masque, P., McGlathery, K. J., Megonigal, J. P., Murdiyarso, D., Russell, B. D., Santos, R., Serrano, O., Silliman, B. R., Watanabe, K., and Duarte, C. M.: The future of Blue Carbon science, *Nature Communications*, 10, 3998, <https://doi.org/10.1038/s41467-019-11693-w>, 2019.
- 850 Mauritsen, T., Bader, J., Becker, T., Behrens, J., Bittner, M., Brokopf, R., Brovkin, V., Claussen, M., Crueger, T., Esch, M., Fast, I., Fiedler, S., Fläschner, D., Gayler, V., Giorgetta, M., Goll, D. S., Haak, H., Hagemann, S., Hedemann, C., Hohenegger, C., Ilyina, T., Jahns, T., Jimenez-de-la Cuesta, D., Jungclaus, J., Kleinen, T., Kloster, S., Kracher, D., Kinne, S., Kleberg, D., Lasslop, G., Kornbluh, L., Marotzke, J., Matei, D., Meraner, K., Mikolajewicz, U., Modali, K., Möbis, B., Müller, W. A., Nabel, J. E. M. S., Nam, C. C. W., Notz, D., Nyawira, S.-S., Paulsen, H., Peters, K., Pincus, R., Pohlmann, H., Pongratz, J., Popp, M., Raddatz, T. J., Rast, S., Redler, R., Reick, C. H., Rohrschneider, T., Schemann, V., Schmidt, H., Schnur, R., Schulzweida, U., Six, K. D., Stein, L., Stemmler, I., Stevens, B., von Storch, J.-S., Tian, F., Voigt, A., Vrese, P., Wieners, K.-H., Wilkenskjaeld, S., Winkler, A., and Roeckner, E.: Developments in the MPI-M Earth System Model version 1.2 (MPI-ESM1.2) and Its Response to Increasing CO<sub>2</sub>, *Journal of Advances in Modeling Earth Systems*, 11, 998–1038, <https://doi.org/10.1029/2018MS001400>, 2019.
- 855 Meehl, G. A., Senior, C. A., Eyring, V., Flato, G., Lamarque, J.-F., Stouffer, R. J., Taylor, K. E., and Schlund, M.: Context for interpreting equilibrium climate sensitivity and transient climate response from the CMIP6 Earth system models, *Science Advances*, 6, eaba1981, <https://doi.org/10.1126/sciadv.aba1981>, 2020.
- 860

- Meinshausen, M., Vogel, E., Nauels, A., Lorbacher, K., Meinshausen, N., Etheridge, D. M., Fraser, P. J., Montzka, S. A., Rayner, P. J., Trudinger, C. M., Krummel, P. B., Beyerle, U., Canadell, J. G., Daniel, J. S., Enting, I. G., Law, R. M., Lunder, C. R., O'Doherty, S., Prinn, R. G., Reimann, S., Rubino, M., Velders, G. J. M., Vollmer, M. K., Wang, R. H. J., and Weiss, R.: Historical greenhouse gas concentrations for climate modelling (CMIP6), *Geoscientific Model Development*, 10, 2057–2116, <https://doi.org/10.5194/gmd-10-2057-2017>, 2017.
- 865 Meinshausen, M., Nicholls, Z. R. J., Lewis, J., Gidden, M. J., Vogel, E., Freund, M., Beyerle, U., Gessner, C., Nauels, A., Bauer, N., Canadell, J. G., Daniel, J. S., John, A., Krummel, P. B., Luderer, G., Meinshausen, N., Montzka, S. A., Rayner, P. J., Reimann, S., Smith, S. J., van den Berg, M., Velders, G. J. M., Vollmer, M. K., and Wang, R. H. J.: The shared socio-economic pathway (SSP) greenhouse gas concentrations and their extensions to 2500, *Geoscientific Model Development*, 13, 3571–3605, <https://doi.org/10.5194/gmd-13-3571-2020>, 2020.
- 870 Muilwijk, M., Nummelin, A., Heuzé, C., Polyakov, I. V., Zanowski, H., and Smedsrud, L. H.: Divergence in Climate Model Projections of Future Arctic Atlantification, *Journal of Climate*, 36, 1727 – 1748, <https://doi.org/10.1175/JCLI-D-22-0349.1>, 2023.
- Myers, N.: Carbon Dioxide Review, *Environmental Conservation*, 10, 370–371, <https://doi.org/10.1017/S0376892900013345>, 1983.
- Nyberg, M. and Hovenden, M. J.: Warming increases soil respiration in a carbon-rich soil without changing microbial respiratory potential, *Biogeosciences*, 17, 4405–4420, <https://doi.org/10.5194/bg-17-4405-2020>, 2020.
- 875 O'Neill, B. C., Tebaldi, C., van Vuuren, D. P., Eyring, V., Friedlingstein, P., Hurtt, G., Knutti, R., Krieglner, E., Lamarque, J.-F., Lowe, J., Meehl, G. A., Moss, R., Riahi, K., and Sanderson, B. M.: The Scenario Model Intercomparison Project (ScenarioMIP) for CMIP6, *Geoscientific Model Development*, 9, 3461–3482, <https://doi.org/10.5194/gmd-9-3461-2016>, 2016.
- Pongratz, J., Reick, C. H., Houghton, R. A., and House, J. I.: Terminology as a key uncertainty in net land use and land cover change carbon flux estimates, *Earth System Dynamics*, 5, 177–195, <https://doi.org/10.5194/esd-5-177-2014>, 2014.
- 880 Raupach, M. R., Gloor, M., Sarmiento, J. L., Canadell, J. G., Frölicher, T. L., Gasser, T., Houghton, R. A., Le Quéré, C., and Trudinger, C. M.: The declining uptake rate of atmospheric CO<sub>2</sub> by land and ocean sinks, *Biogeosciences*, 11, 3453–3475, <https://doi.org/10.5194/bg-11-3453-2014>, 2014.
- Resplandy, L., Keeling, R., Rödenbeck, C., Stephens, B. B., Khatiwala, S., Rodgers, K., Long, M. C., Bopp, L., and Tans, P. P.: Revision of global carbon fluxes based on a reassessment of oceanic and riverine carbon transport, *Nature Geoscience*, 11, 504–509, <https://doi.org/10.1038/s41561-018-0151-3>, 2018.
- 885 Riahi, K., van Vuuren, D. P., Krieglner, E., Edmonds, J., O'Neill, B. C., Fujimori, S., Bauer, N., Calvin, K., Dellink, R., Fricko, O., Lutz, W., Popp, A., Cuaresma, J. C., KC, S., Leimbach, M., Jiang, L., Kram, T., Rao, S., Emmerling, J., Ebi, K., Hasegawa, T., Havlik, P., Humpenöder, F., Da Silva, L. A., Smith, S., Stehfest, E., Bosetti, V., Eom, J., Gernaat, D., Masui, T., Rogelj, J., Strefler, J., Drouet, L., Krey, V., Luderer, G., Harmsen, M., Takahashi, K., Baumstark, L., Doelman, J. C., Kainuma, M., Klimont, Z., Marangoni, G., Lotze-Campen, H., Obersteiner, M., Tabeau, A., and Tavoni, M.: The Shared Socioeconomic Pathways and their energy, land use, and greenhouse gas emissions implications: An overview, *Global Environmental Change*, 42, 153–168, <https://doi.org/10.1016/j.gloenvcha.2016.05.009>, 2017.
- 890 Righi, M., Andela, B., Eyring, V., Lauer, A., Predoi, V., Schlund, M., Vegas-Regidor, J., Bock, L., Brötz, B., de Mora, L., Diblen, F., Dreyer, L., Drost, N., Earnshaw, P., Hassler, B., Koldunov, N., Little, B., Loosveldt Tomas, S., and Zimmermann, K.: Earth System Model Evaluation Tool (ESMValTool) v2.0 – technical overview, *Geoscientific Model Development*, 13, 1179–1199, <https://doi.org/10.5194/gmd-13-1179-2020>, 2020.
- Roser, M. and Ritchie, H.: Oil Spills, *Our World in Data*, <https://ourworldindata.org/oil-spills>, Accessed: 2023-09-11, 2023.



- Sallée, J.-B., Pellichero, V., Akhoudas, C., Pauthenet, E., Vignes, L., Schmidtko, S., Garabato, A. N., Sutherland, P., and Kuusela, M.:  
Summertime increases in upper-ocean stratification and mixed-layer depth, *Nature*, 591, 592–598, <https://doi.org/10.1038/s41586-021-03303-x>, 2021.
- Scafetta, N.: Advanced Testing of Low, Medium, and High ECS CMIP6 GCM Simulations Versus ERA5-T2m, *Geophysical Research Letters*, 49, e2022GL097716, <https://doi.org/10.1029/2022GL097716>, 2022.
- Schlunegger, S., Rodgers, K. B., Sarmiento, J. L., Frölicher, T. L., Dunne, J. P., Ishii, M., and Slater, R.: Emergence of anthropogenic signals in the ocean carbon cycle, *Nature Climate Change*, 9, 719–725, <https://doi.org/10.1038/s41558-019-0553-2>, 2019.
- 905 Sellar, A. A., Walton, J., Jones, C. G., Wood, R., Abraham, N. L., Andrejczuk, M., Andrews, M. B., Andrews, T., Archibald, A. T., de Mora, L., Dyson, H., Elkington, M., Ellis, R., Florek, P., Good, P., Gohar, L., Haddad, S., Hardiman, S. C., Hogan, E., Iwi, A., Jones, C. D., Johnson, B., Kelley, D. I., Kettleborough, J., Knight, J. R., Köhler, M. O., Kuhlbrodt, T., Liddicoat, S., Linova-Pavlova, I., Mizieliński, M. S., Morgenstern, O., Mulcahy, J., Neining, E., O’Connor, F. M., Petrie, R., Ridley, J., Rioual, J.-C., Roberts, M., Robertson, E., Rumbold, S., Seddon, J., Shepherd, H., Shim, S., Stephens, A., Teixeira, J. C., Tang, Y., Williams, J., Wiltshire, A., and Griffiths, P. T.: Implementation of U.K. Earth System Models for CMIP6, *Journal of Advances in Modeling Earth Systems*, 12, e2019MS001946, <https://doi.org/10.1029/2019MS001946>, 2020.
- 910 Sherwood, S. C., Webb, M. J., Annan, J. D., Armour, K. C., Forster, P. M., Hargreaves, J. C., Hegerl, G., Klein, S. A., Marvel, K. D., Rohling, E. J., Watanabe, M., Andrews, T., Braconnot, P., Bretherton, C. S., Foster, G. L., Hausfather, Z., von der Heydt, A. S., Knutti, R., Mauritsen, T., Norris, J. R., Proistosescu, C., Rugenstein, M., Schmidt, G. A., Tokarska, K. B., and Zelinka, M. D.: An Assessment of Earth’s Climate Sensitivity Using Multiple Lines of Evidence, *Reviews of Geophysics*, 58, e2019RG000678, <https://doi.org/10.1029/2019RG000678>, 2020.
- Smith, C. J., Kramer, R. J., Myhre, G., Alterskjær, K., Collins, W., Sima, A., Boucher, O., Dufresne, J.-L., Nabat, P., Michou, M., Yukimoto, S., Cole, J., Paynter, D., Shiogama, H., O’Connor, F. M., Robertson, E., Wiltshire, A., Andrews, T., Hannay, C., Miller, R., Nazarenko, L., Kirkevåg, A., Olivíé, D., Fiedler, S., Lewinschal, A., Mackallah, C., Dix, M., Pincus, R., and Forster, P. M.: Effective radiative forcing and adjustments in CMIP6 models, *Atmospheric Chemistry and Physics*, 20, 9591–9618, <https://doi.org/10.5194/acp-20-9591-2020>, 2020.
- 920 Sullivan, A., Baker, E., and Kurvits, T.: Spreading Like Wildfire: The Rising Threat of Extraordinary Landscape Fires, Tech. rep., UN Environment Program, [https://policycommons.net/artifacts/2259313/wildfire\\_rra](https://policycommons.net/artifacts/2259313/wildfire_rra), accessed 2023-09-11, 2022.
- Swaminathan, R., Parker, R. J., Jones, C. G., Allan, R. P., Quaife, T., Kelley, D. I., de Mora, L., and Walton, J.: The Physical Climate at Global Warming Thresholds as Seen in the U.K. Earth System Model, *Journal of Climate*, 35, 29 – 48, <https://doi.org/10.1175/JCLI-D-21-0234.1>, 2022.
- 925 Swart, N. C., Cole, J. N. S., Kharin, V. V., Lazare, M., Scinocca, J. F., Gillett, N. P., Anstey, J., Arora, V., Christian, J. R., Hanna, S., Jiao, Y., Lee, W. G., Majaess, F., Saenko, O. A., Seiler, C., Seinen, C., Shao, A., Sigmond, M., Solheim, L., von Salzen, K., Yang, D., and Winter, B.: The Canadian Earth System Model version 5 (CanESM5.0.3), *Geoscientific Model Development*, 12, 4823–4873, <https://doi.org/10.5194/gmd-12-4823-2019>, 2019.
- 930 Tebaldi, C., Debeire, K., Eyring, V., Fischer, E., Fyfe, J., Friedlingstein, P., Knutti, R., Lowe, J., O’Neill, B., Sanderson, B., van Vuuren, D., Riahi, K., Meinshausen, M., Nicholls, Z., Tokarska, K. B., Hurtt, G., Kriegler, E., Lamarque, J.-F., Meehl, G., Moss, R., Bauer, S. E., Boucher, O., Brovkin, V., Byun, Y.-H., Dix, M., Gualdi, S., Guo, H., John, J. G., Kharin, S., Kim, Y., Koshiro, T., Ma, L., Olivíé, D., Panickal, S., Qiao, F., Rong, X., Rosenbloom, N., Schupfner, M., Séférian, R., Sellar, A., Semmler, T., Shi, X., Song, Z., Steger, C., Stouffer, R., Swart, N., Tachiiri, K., Tang, Q., Tatebe, H., Voldoire, A., Volodin, E., Wyser, K., Xin, X., Yang, S., Yu, Y., and Ziehn,

- 935 T.: Climate model projections from the Scenario Model Intercomparison Project (ScenarioMIP) of CMIP6, *Earth System Dynamics*, 12, 253–293, <https://doi.org/10.5194/esd-12-253-2021>, 2021.
- Thibodeau, B., Not, C., Zhu, J., Schmittner, A., Noone, D., Tabor, C., Zhang, J., and Liu, Z.: Last Century Warming Over the Canadian Atlantic Shelves Linked to Weak Atlantic Meridional Overturning Circulation, *Geophysical Research Letters*, 45, 12,376–12,385, <https://doi.org/10.1029/2018GL080083>, 2018.
- 940 Twomey, S.: The Influence of Pollution on the Shortwave Albedo of Clouds, *Journal of Atmospheric Sciences*, 34, 1149 – 1152, [https://doi.org/10.1175/1520-0469\(1977\)034<1149:TIOPOP>2.0.CO;2](https://doi.org/10.1175/1520-0469(1977)034<1149:TIOPOP>2.0.CO;2), 1977.
- Ukkola, A. M., Prentice, I., Keenan, T. F., van Dijk, A. I., Viney, N. R., Myneni, R., and Bi, J.: Reduced streamflow in water-stressed climates consistent with CO<sub>2</sub> effects on vegetation, *Nature Climate Change*, 6, 75–78, <https://doi.org/10.1038/nclimate2831>, 2016.
- United Nations: Transforming our world : the 2030 Agenda for Sustainable Development, p. 35 p., <http://digitallibrary.un.org/record/3923923>, issued in GAOR, 70th sess., Suppl. no. 49., 2015.
- 945 United Nations Environment Programme: Emissions Gap Report 2019, <https://wedocs.unep.org/20.500.11822/30797>, accessed 2023-09-11, 2019.
- United Nations Treaty Collection: Paris Agreement, [https://treaties.un.org/pages/ViewDetails.aspx?src=TREATY&mtdsg\\_no=XXVII-7-d&chapter=27&clang=\\_en](https://treaties.un.org/pages/ViewDetails.aspx?src=TREATY&mtdsg_no=XXVII-7-d&chapter=27&clang=_en), 2015.
- 950 van der Molen, M., Dolman, A., Ciais, P., Eglin, T., Gobron, N., Law, B., Meir, P., Peters, W., Phillips, O., Reichstein, M., Chen, T., Dekker, S., Doubková, M., Friedl, M., Jung, M., van den Hurk, B., de Jeu, R., Kruijt, B., Ohta, T., Rebel, K., Plummer, S., Seneviratne, S., Sitch, S., Teuling, A., van der Werf, G., and Wang, G.: Drought and ecosystem carbon cycling, *Agricultural and Forest Meteorology*, 151, 765–773, <https://doi.org/10.1016/j.agrformet.2011.01.018>, 2011.
- Wang, S., Zhang, Y., Ju, W., Chen, J. M., Ciais, P., Cescatti, A., Sardans, J., Janssens, I. A., Wu, M., Berry, J. A., Campbell, E., Fernández-Martínez, M., Alkama, R., Sitch, S., Friedlingstein, P., Smith, W. K., Yuan, W., He, W., Lombardozzi, D., Kautz, M., Zhu, D., Lienert, S., Kato, E., Poulter, B., Sanders, T. G. M., Krüger, I., Wang, R., Zeng, N., Tian, H., Vuichard, N., Jain, A. K., Wiltshire, A., Haverd, V., Goll, D. S., and Peñuelas, J.: Recent global decline of CO<sub>2</sub> fertilization effects on vegetation photosynthesis, *Science*, 370, 1295–1300, <https://doi.org/10.1126/science.abb7772>, 2020.
- 955 Watson, A. J., Schuster, U., Shutler, J. D., Holding, T., Ashton, I. G. C., Landschützer, P., Woolf, D. K., and Goddijn-Murphy, L.: Revised estimates of ocean-atmosphere CO<sub>2</sub> flux are consistent with ocean carbon inventory, *Nature Communications*, 11, 4422, <https://doi.org/10.1038/s41467-020-18203-3>, 2020.
- 960 Weijer, W., Cheng, W., Garuba, O. A., Hu, A., and Nadiga, B. T.: CMIP6 Models Predict Significant 21st Century Decline of the Atlantic Meridional Overturning Circulation, *Geophysical Research Letters*, 47, e2019GL086075, <https://doi.org/10.1029/2019GL086075>, 2020.
- World Bank: Turn Down the Heat: Why a 4°C Warmer World Must Be Avoided, <http://documents.worldbank.org/curated/en/865571468149107611/Turn-down-the-heat-why-a-4-C-warmer-world-must-be-avoided>, accessed 2023-09-11, 2012.
- 965 Yool, A., Palmiéri, J., Jones, C. G., Sellar, A. A., de Mora, L., Kuhlbrodt, T., Popova, E. E., Mulcahy, J. P., Wiltshire, A., Rumbold, S. T., Stringer, M., Hill, R. S. R., Tang, Y., Walton, J., Blaker, A., Nurser, A. J. G., Coward, A. C., Hirschi, J., Woodward, S., Kelley, D. I., Ellis, R., and Rumbold-Jones, S.: Spin-up of UK Earth System Model 1 (UKESM1) for CMIP6, *Journal of Advances in Modeling Earth Systems*, 12, e2019MS001933, <https://doi.org/10.1029/2019MS001933>, 2020.
- 970 Zeebe, R. E.: History of Seawater Carbonate Chemistry, Atmospheric CO<sub>2</sub>, and Ocean Acidification, *Annual Review of Earth and Planetary Sciences*, 40, 141–165, <https://doi.org/10.1146/annurev-earth-042711-105521>, 2012.

- Zelinka, M. D., Myers, T. A., McCoy, D. T., Po-Chedley, S., Caldwell, P. M., Ceppi, P., Klein, S. A., and Taylor, K. E.: Causes of Higher Climate Sensitivity in CMIP6 Models, *Geophysical Research Letters*, 47, e2019GL085782, <https://doi.org/10.1029/2019GL085782>, 2020.
- 975 Ziehn, T., Chamberlain, M. A., Law, R. M., Lenton, A., Bodman, R. W., Dix, M., Stevens, L., Wang, Y.-P., and Srbinovsky, J.: The Australian Earth System Model: ACCESS-ESM1.5, *Journal of Southern Hemisphere Earth Systems Science*, 70, 193–214, <https://doi.org/10.1071/ES19035>, 2020.